ZAMM · Z. Angew. Math. Mech. **95**, No. 9, 911 – 938 (2015) / **DOI** 10.1002/zamm.201300191

# Predictor/corrector co-simulation approaches for solver coupling with algebraic constraints

**Bernhard Schweizer*** **and Daixing Lu**

Department of Mechanical Engineering, Institute of Structural Dynamics, Technical University Darmstadt, Germany

Received 29 August 2013, revised 28 January 2014, accepted 26 February 2014
Published online 12 May 2014

**Key words** Co-simulation, solver coupling, subcycling, algebraic constraints, predictor/corrector approach, semi-implicit.

In the paper at hand, co-simulation approaches are analyzed for coupling two solvers. The solvers are assumed to be coupled by algebraic constraint equations. We discuss 2 different coupling methods. Both methods are semi-implicit, i.e. they are based on a predictor/corrector approach. Method 1 makes use of the well-known Baumgarte-stabilization technique. Method 2 is based on a weighted multiplier approach. For both methods, we investigate formulations on index-3, index-2 and index-1 level and analyze the convergence, the numerical stability and the numerical error. The presented approaches require Jacobian matrices. Since only partial derivatives with respect to the coupling variables are needed, calculation of the Jacobian matrices may very easily be calculated numerically and in parallel with the predictor step. For that reason, the presented methods can in a straightforward manner be applied to couple commercial simulation tools without full solver access. The only requirement on the subsystem solvers is that the macro-time step can be repeated once in order to accomplish the corrector step. Within the paper, we introduce methods for coupling mechanical systems. The presented approaches can, however, also be applied to couple arbitrary non-mechanical dynamical systems.



## 1 Introduction

Co-simulation – also called solver or simulator coupling – is a frequently used numerical technique to couple two or more solvers in time domain. One major field of application for co-simulation methods is the analysis of multidisciplinary problems. Usually, specialized simulation codes exist for different physical disciplines (e.g. FEM codes for structural dynamics analyses, CFD codes for fluid dynamic problems or multibody codes for the dynamic analysis of mechanisms). In order to simulate a coupled multidisciplinary problem, the different codes can be coupled by means of an appropriate co-simulation approach. Simulator coupling has, for instance, been successfully applied in the field of fluid/structure interaction [1, 2, 11], for coupling multibody and hydraulic systems [6, 18] or in the field of electrical circuit simulation [28]. Solver coupling may, however, also be used to analyze monodisciplinary problems in order to parallelize the simulation process [5, 13].

For solver coupling, different techniques have been developed, see for instance [8, 12, 15, 20, 22, 25–27]. Two main strategies have to be distinguished. On the one hand, two mechanical subsystems can be coupled by applied forces/torques. In this case, the subsystems are coupled by physical force/torque laws [7, 9, 10, 14, 18, 19, 23]. On the other hand, two subsystems can be coupled by reaction forces/torques. Then, solver coupling is accomplished on the basis of algebraic constraint equations [3, 16, 21]. In this manuscript, we only consider constraint coupling.

Constraint coupling has been investigated by different authors. Usually, implicit or semi-implicit coupling schemes are used in connection with constraint coupling [3, 21]. However, also explicit schemes have been developed in order to couple two subsystems with algebraic constraints. In [16], for instance, an explicit coupling scheme on index-1 level has been analyzed for the case of constant approximation polynomials. Implicit coupling schemes often require Jacobian matrices. The Jacobian matrices of the methods analyzed here have very small dimensions, since only partial derivatives of the state vectors of the two coupling bodies with respect to the coupling variables are necessary. Since the approaches presented here are semi-implicit, the macro-time step has to be repeated once, i.e. the subsystem solvers have to be reinitialized at the previous macro-time point.

Compared with other approaches for solver coupling with algebraic constraints known from literature, the methods presented here have certain advantages and disadvantages. In comparison with the explicit method of [16] (index-1 approach with constant approximation), the here discussed predictor/corrector approaches show a significantly better stability

* Corresponding author E-mail: schweizer@sds.tu-darmstadt.de, Phone: +49-6151-16-3461, Fax: +49-6151-16-3668

behavior, see Sect. 4, even for the important case that higher order approximation is used. Also, index-2 and index-3 formulations show numerically stable results. Besides the improved numerical stability, the predictor/corrector approaches usually yield more accurate results. The drawback of the predictor/corrector approaches compared with the explicit method is that implementation is more involved, since the macro-time step has to be repeated once. Compared with the sequential method presented in [3], the predictor/corrector approaches can be fully parallelized, which may significantly speed up the simulation time. To guarantee convergence for the sequential method in [3], either a special contractivity condition has to be fulfilled or special stabilization techniques have to be applied to achieve stable results. For the stabilization technique proposed in [3], for instance, a projection step is required in each macro-time step, for which detailed subsystem information (mass and Jacobian matrices) has to be provided. The here proposed methods do not need any detailed subsystem information, which may from the practical point of view be an important advantage, especially for the case that commercial simulation codes have to be coupled. Constraint coupling is also investigated in [21]. The example discussed in [21] is based on an index-1 approach, and it is shown that stable results are in general only achieved if an iterative scheme is applied. In comparison to the methods examined in [3,21], the presented predictor/corrector approaches have the advantage that – by using predicted and corrected variables – an error estimator and a variable macro-step size can be implemented in a very straightforward manner. One drawback of the presented methods compared to the methods in [3, 21] is that for the index-2 and index-1 formulations user-defined parameters have to be specified (one parameter in the index-2 case and two parameters in the index-1 case). Since the predictor/corrector approaches show a good stability behavior, proper choice of these parameters seems to be unproblematic.

Starting point of a co-simulation approach is the overall physical system. This overall system is decomposed into two (or more) subsystems. Here, we only consider the case of two subsystems. To couple the subsystems, coupling variables have to be defined in each subsystem. We assume that each subsystem has its own solver, which integrates independently from the solver of the other subsystem. In the framework of a co-simulation approach (weak coupling approach), a macro-time grid – also called communication-time grid – has to be defined, i.e. we have to specify macro-time points $T_0, T_1, \ldots, T_N$. In this paper, we restrict ourselves on equidistant macro-time grids, i.e. the macro-step size $H = T_{N+1} - T_N$ is assumed to be constant. Between the macro-time points, the subsystems integrate independently from each other. At the macro-time points, the coupling variables are exchanged between the subsystems. In order to perform the subsystem integration from $T_N$ to $T_{N+1}$, the coupling variables have to be approximated in the subsystems. In the predictor step, coupling variables are extrapolated, whereas interpolation is used in the corrector step.

This manuscript is arranged as follows: in Sect. 2, we briefly introduce the 2 methods by means of a simple co-simulation test model. The approaches are generalized for coupling arbitrary mechanical subsystems with rather general coupling conditions (i.e. arbitrary rigid joints) in Sect. 3. The convergence behavior and the numerical stability of the 2 methods are investigated in Sect. 4. An alternative approach to calculate the partial derivatives for the Jacobian matrices is discussed in Appendix A and a simplified formulation of the coupling scheme is sketched in Appendix B (see Supplementary Material in Wiley online library).

It should finally be mentioned that the co-simulation test model in Sect. 2 as well as the mechanical models considered in Sects. 4.2 and 4.3 are simple and pure mechanical models, which would usually be solved directly without applying any co-simulation technique. To investigate convergence and numerical error of different co-simulation approaches, simple test models are very useful and frequently applied in literature [14,21,27]. The methods introduced in this paper can however be applied to arbitrary multibody or structural dynamics systems. The application to non-mechanical systems is also possible and can be accomplished in a very similar way.

## 2 Predictor/corrector co-simulation approaches for linear test model

We consider the probably most simple co-simulation test model for constraint coupling, namely the linear 1-DOF oscillator depicted in Fig. 1. This test model consists of two single mass oscillators (masses $m_1/m_2$, spring constants $c_1/c_2$, damping coefficients $d_1/d_2$), which are connected by a rigid massless link. Hence, the test model may be interpreted as two single-mass oscillators, coupled by the algebraic constraint $x_2 - x_1 = 0$. The position of the two masses is described by the coordinates $x_1/x_2$ and the corresponding velocities by $v_1/v_2$. The springs are assumed to be stress-free for $x_1 = x_2 = 0$. The equations of motion (index-3 DAE system) for the autonomous system read as

$$\begin{aligned}
\dot{x_1} &= v_1\,, \qquad \dot{v_1} = -\frac{c_1}{m_1}x_1 - \frac{d_1}{m_1}v_1 + \frac{\lambda_c}{m_1}\,,\\
\dot{x_2} &= v_2\,, \qquad \dot{v_2} = -\frac{c_2}{m_2}x_2 - \frac{d_2}{m_2}v_2 - \frac{\lambda_c}{m_2}\,,\\
g_{c\lambda} &:= x_2 - x_1 = 0\,.
\end{aligned} \tag{1}$$

 

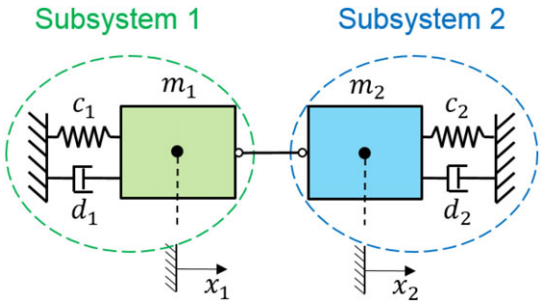


**Fig. 1** Linear 1-DOF oscillator: interpretation as two coupled single-mass oscillators.

In the above equations, $\lambda_c$ denotes the Lagrange multiplier. The initial conditions for the state variables are given by

$$x_1(t=0) = x_{1,0} = x_0\,, \qquad v_1(t=0) = v_{1,0} = v_0\,,$$
$$x_2(t=0) = x_{2,0} = x_0\,, \qquad v_2(t=0) = v_{2,0} = v_0\,. \tag{2}$$

Based on the initial conditions (2), the initial condition for $\lambda_c$ is determined by

$$\lambda_c(t=0) = \lambda_{c,0} = \frac{m_1 \cdot m_2}{m_1 + m_2} \cdot \left[ \left( \frac{c_1}{m_1} - \frac{c_2}{m_2} \right) \cdot x_0 + \left( \frac{d_1}{m_1} - \frac{d_2}{m_2} \right) \cdot v_0 \right]. \tag{3}$$

### 2.1 Method 1: Semi-implicit co-simulation approach based on Baumgarte-stabilization

The first method makes use of the Baumgarte-stabilization technique in order to calculate corrected coupling variables for the corrector step. Applying a co-simulation approach, the overall system 1 is split into two subsystems. Here, the overall system 1 is decomposed into two subsystems so that both subsystems are force-driven single-mass oscillators, see Fig. 2. The single-mass oscillators are excited by the coupling (constraint) force $\lambda_c$.

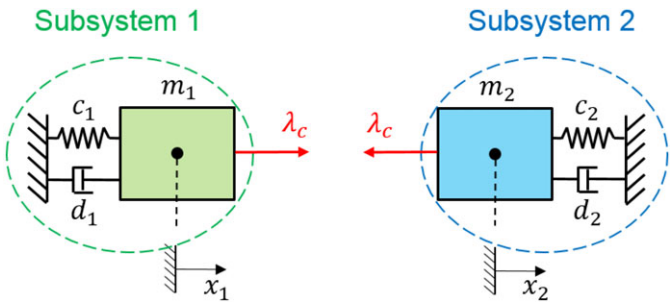


**Fig. 2** Decomposed 1-DOF oscillator.

The decomposed 1-DOF oscillator is described by the following equations

Subsystem 1:

$$\dot{x}_1 = v_1\,, \qquad \dot{v}_1 = -\frac{c_1}{m_1} x_1 - \frac{d_1}{m_1} v_1 + \frac{\lambda_c}{m_1}\,, \tag{4a}$$

Subsystem 2:

$$\dot{x}_2 = v_2\,, \qquad \dot{v}_2 = -\frac{c_2}{m_2} x_2 - \frac{d_2}{m_2} v_2 - \frac{\lambda_c}{m_2}\,, \tag{4b}$$

Coupling condition:

$$g_{c\lambda}^B := (x_2 - x_1) + \beta \cdot (v_2 - v_1) + \gamma \cdot (\dot{v}_2 - \dot{v}_1) = 0\,. \tag{4c}$$

In order to reduce the index of the DAE system, we use the well-known Baumgarte-stabilization method [4], i.e. we replace the constraint equation $g_{c\lambda} := x_2 - x_1 = 0$ in Eq. (1) by the coupling equation (4c). Note that $\beta \geq 0$ and $\gamma \geq 0$ are real-valued user-defined parameters (e.g. $\beta = 2E-3$ and $\gamma = 1E-6$).

To explain the semi-implicit co-simulation approach, we consider the general macro-time step from $T_N$ to $T_{N+1}$. In order to describe the method quite briefly and clearly, we restrict ourselves in Sect. 2 to the case that constant approximation is

 

used for extrapolating/interpolating the coupling force $\lambda_c$. Approximation with higher order polynomials is discussed in Sect. 3. The semi-implicit method is accomplished in 3 steps, which are described below.

At the beginning of the macro-time step, the state variables and the coupling variable are assumed to be known

$$\begin{aligned} &x_1(t=T_N) = x_{1,N}\,, \qquad v_1(t=T_N) = v_{1,N}\,, \\ &x_2(t=T_N) = x_{2,N}\,, \qquad v_2(t=T_N) = v_{2,N}\,, \end{aligned} \tag{5a}$$

$$\lambda_c(t=T_N) = \lambda_{c,N}\,. \tag{5b}$$

**Step 1: Predictor step**

- Using the predicted (extrapolated) coupling force

$$\lambda_c^p(t) = \lambda_{c,N+1}^p = \lambda_{c,N} = \text{const}\,, \tag{6}$$

the integration of subsystem 1 and subsystem 2 from $T_N$ to $T_{N+1}$ with the initial conditions (5a) yields the predicted state variables at the macro-time point $T_{N+1}$

$$\begin{aligned} &x_{1,N+1}^p = x_{1,N+1}(\lambda_{c,N+1}^p)\,, \qquad v_{1,N+1}^p = v_{1,N+1}(\lambda_{c,N+1}^p)\,, \\ &x_{2,N+1}^p = x_{2,N+1}(\lambda_{c,N+1}^p)\,, \qquad v_{2,N+1}^p = v_{2,N+1}(\lambda_{c,N+1}^p)\,. \end{aligned} \tag{7}$$

Inserting the predicted state variables from Eq. (7) into the equations of motion (4a) and (4b) yields the predicted accelerations at the macro-time point $T_{N+1}$

$$\dot{v}_{1,N+1}^p = \dot{v}_{1,N+1}(\lambda_{c,N+1}^p)\,, \qquad \dot{v}_{2,N+1}^p = \dot{v}_{2,N+1}(\lambda_{c,N+1}^p)\,. \tag{8}$$

It should be stressed that for the simple case of constant extrapolation in the time interval $[T_N, T_{N+1}]$, the predicted coupling force $\lambda_c^p(t)$ equals the corrected coupling force $\lambda_{c,N}$ at the previous macro-time point $T_N$.

**Step 2: Calculation of corrected coupling force**

- Using the perturbed predicted coupling force

$$\lambda_{c,N+1}^{pp_\lambda} = \lambda_{c,N+1}^p + \Delta\lambda_c = \text{const}\,, \tag{9}$$

the integration of subsystem 1 and subsystem 2 from $T_N$ to $T_{N+1}$ with the initial conditions (5a) yields the perturbed predicted state variables at the macro-time point $T_{N+1}$

$$\begin{aligned} &x_{1,N+1}^{pp_\lambda} = x_{1,N+1}(\lambda_{c,N+1}^{pp_\lambda})\,, \qquad v_{1,N+1}^{pp_\lambda} = v_{1,N+1}(\lambda_{c,N+1}^{pp_\lambda})\,, \\ &x_{2,N+1}^{pp_\lambda} = x_{2,N+1}(\lambda_{c,N+1}^{pp_\lambda})\,, \qquad v_{2,N+1}^{pp_\lambda} = v_{2,N+1}(\lambda_{c,N+1}^{pp_\lambda})\,. \end{aligned} \tag{10}$$

Inserting the perturbed predicted state variables from Eq. (10) into the equations of motion (4a) and (4b) yields the perturbed predicted accelerations at the macro-time point $T_{N+1}$

$$\dot{v}_{1,N+1}^{pp_\lambda} = \dot{v}_{1,N+1}(\lambda_{c,N+1}^{pp_\lambda})\,, \qquad \dot{v}_{2,N+1}^{pp_\lambda} = \dot{v}_{2,N+1}(\lambda_{c,N+1}^{pp_\lambda})\,. \tag{11}$$

It should be mentioned that $\Delta\lambda_c$ is a user-defined increment.

- With the predicted and the perturbed predicted state variables and accelerations, the partial derivatives of the states and accelerations with respect to the coupling force can approximately be calculated by finite differences

 

$$
\begin{aligned}
\left.\frac{\partial x_{1,N+1}}{\partial \lambda_{c,N+1}}\right|_{\lambda^p_{c,N+1}} &= \lim_{\Delta\lambda_c\to 0} \frac{x_{1,N+1}(\lambda^p_{c,N+1}+\Delta\lambda_c) - x_{1,N+1}(\lambda^p_{c,N+1})}{\Delta\lambda_c} \approx \frac{x^{pp_\lambda}_{1,N+1} - x^p_{1,N+1}}{\Delta\lambda_c}\,,\\
\left.\frac{\partial v_{1,N+1}}{\partial \lambda_{c,N+1}}\right|_{\lambda^p_{c,N+1}} &= \lim_{\Delta\lambda_c\to 0} \frac{v_{1,N+1}(\lambda^p_{c,N+1}+\Delta\lambda_c) - v_{1,N+1}(\lambda^p_{c,N+1})}{\Delta\lambda_c} \approx \frac{v^{pp_\lambda}_{1,N+1} - v^p_{1,N+1}}{\Delta\lambda_c}\,,\\
\left.\frac{\partial \dot v_{1,N+1}}{\partial \lambda_{c,N+1}}\right|_{\lambda^p_{c,N+1}} &= \lim_{\Delta\lambda_c\to 0} \frac{\dot v_{1,N+1}(\lambda^p_{c,N+1}+\Delta\lambda_c) - \dot v_{1,N+1}(\lambda^p_{c,N+1})}{\Delta\lambda_c} \approx \frac{\dot v^{pp_\lambda}_{1,N+1} - \dot v^p_{1,N+1}}{\Delta\lambda_c}\,,\\
\left.\frac{\partial x_{2,N+1}}{\partial \lambda_{c,N+1}}\right|_{\lambda^p_{c,N+1}} &= \lim_{\Delta\lambda_c\to 0} \frac{x_{2,N+1}(\lambda^p_{c,N+1}+\Delta\lambda_c) - x_{2,N+1}(\lambda^p_{c,N+1})}{\Delta\lambda_c} \approx \frac{x^{pp_\lambda}_{2,N+1} - x^p_{2,N+1}}{\Delta\lambda_c}\,,\\
\left.\frac{\partial v_{2,N+1}}{\partial \lambda_{c,N+1}}\right|_{\lambda^p_{c,N+1}} &= \lim_{\Delta\lambda_c\to 0} \frac{v_{2,N+1}(\lambda^p_{c,N+1}+\Delta\lambda_c) - v_{2,N+1}(\lambda^p_{c,N+1})}{\Delta\lambda_c} \approx \frac{v^{pp_\lambda}_{2,N+1} - v^p_{2,N+1}}{\Delta\lambda_c}\,,\\
\left.\frac{\partial \dot v_{2,N+1}}{\partial \lambda_{c,N+1}}\right|_{\lambda^p_{c,N+1}} &= \lim_{\Delta\lambda_c\to 0} \frac{\dot v_{2,N+1}(\lambda^p_{c,N+1}+\Delta\lambda_c) - \dot v_{2,N+1}(\lambda^p_{c,N+1})}{\Delta\lambda_c} \approx \frac{\dot v^{pp_\lambda}_{2,N+1} - \dot v^p_{2,N+1}}{\Delta\lambda_c}\,.
\end{aligned}
\tag{12}
$$

- Making use of the partial derivatives, an improved (corrected) value for the coupling force can be computed. With this improved coupling force the macro-time step $T_N \rightarrow T_{N+1}$ is repeated in the corrector step. For calculating the corrected coupling force, we consider the coupling condition $g^B_{c\lambda,N+1}$ at the fixed time point $T_{N+1}$ and interpret $g^B_{c\lambda,N+1}$ as a function of the coupling force $\lambda_{c,N+1}$

$$
\begin{aligned}
g^B_{c\lambda,N+1}(\lambda_{c,N+1}) := &\big(x_{2,N+1}(\lambda_{c,N+1}) - x_{1,N+1}(\lambda_{c,N+1})\big)\\
&+\beta\cdot\big(v_{2,N+1}(\lambda_{c,N+1}) - v_{1,N+1}(\lambda_{c,N+1})\big)\\
&+\gamma\cdot\big(\dot v_{2,N+1}(\lambda_{c,N+1}) - \dot v_{1,N+1}(\lambda_{c,N+1})\big)\,.
\end{aligned}
\tag{13}
$$

Next, the function $g^B_{c\lambda,N+1}(\lambda_{c,N+1})$ is expanded in a Taylor series with respect to $\lambda_{c,N+1}$. As expansion point, we choose $\lambda^p_{c,N+1}$. Neglecting the higher order terms $\mathcal{O}(\lambda^2_{c,N+1})$, a Taylor series expansion of $g^B_{c\lambda,N+1}(\lambda_{c,N+1})$ yields the linearized coupling condition

$$
\begin{aligned}
g^{B,linear}_{c\lambda,N+1}(\lambda_{c,N+1}) :=& g^B_{c\lambda,N+1}(\lambda^p_{c,N+1}) + \left.\frac{\partial g^B_{c\lambda,N+1}}{\partial\lambda_{c,N+1}}\right|_{\lambda^p_{c,N+1}}\cdot(\lambda_{c,N+1}-\lambda^p_{c,N+1})\\
=&\Big(x_{2,N+1}(\lambda^p_{c,N+1}) - x_{1,N+1}(\lambda^p_{c,N+1})\Big)\\
&+\beta\cdot\Big(v_{2,N+1}(\lambda^p_{c,N+1}) - v_{1,N+1}(\lambda^p_{c,N+1})\Big)\\
&+\gamma\cdot\Big(\dot v_{2,N+1}(\lambda^p_{c,N+1}) - \dot v_{1,N+1}(\lambda^p_{c,N+1})\Big)\\
&+\Bigg[\left(\left.\frac{\partial x_{2,N+1}}{\partial\lambda_{c,N+1}}\right|_{\lambda^p_{c,N+1}} - \left.\frac{\partial x_{1,N+1}}{\partial\lambda_{c,N+1}}\right|_{\lambda^p_{c,N+1}}\right)\\
&+\beta\cdot\left(\left.\frac{\partial v_{2,N+1}}{\partial\lambda_{c,N+1}}\right|_{\lambda^p_{c,N+1}} - \left.\frac{\partial v_{1,N+1}}{\partial\lambda_{c,N+1}}\right|_{\lambda^p_{c,N+1}}\right)\\
&+\gamma\cdot\left(\left.\frac{\partial \dot v_{2,N+1}}{\partial\lambda_{c,N+1}}\right|_{\lambda^p_{c,N+1}} - \left.\frac{\partial \dot v_{1,N+1}}{\partial\lambda_{c,N+1}}\right|_{\lambda^p_{c,N+1}}\right)\Bigg]\cdot(\lambda_{c,N+1}-\lambda^p_{c,N+1}) = 0\,.
\end{aligned}
\tag{14}
$$

- Generally, the predicted states and accelerations do not fulfill the coupling condition, i.e. $g^B_{c\lambda,N+1}(\lambda^p_{c,N+1}) := \Big(x_{2,N+1}(\lambda^p_{c,N+1}) - x_{1,N+1}(\lambda^p_{c,N+1})\Big) + \beta\cdot\Big(v_{2,N+1}(\lambda^p_{c,N+1}) - v_{1,N+1}(\lambda^p_{c,N+1})\Big)$ $+\gamma\cdot\Big(\dot v_{2,N+1}(\lambda^p_{c,N+1}) - \dot v_{1,N+1}(\lambda^p_{c,N+1})\Big) \neq 0$. An improved (corrected) coupling force, which at least fulfills the

linearized coupling condition (14), can be derived by solving Eq. (14) for $\lambda_{c,N+1}$. The result is

$$\lambda_{c,N+1} = \lambda^p_{c,N+1} - \frac{\left(x_{2,N+1}(\lambda^p_{c,N+1}) - x_{1,N+1}(\lambda^p_{c,N+1})\right) + \beta \cdot \left(v_{2,N+1}(\lambda^p_{c,N+1}) - v_{1,N+1}(\lambda^p_{c,N+1})\right) + \cdots}{\left(\left.\frac{\partial x_{2,N+1}}{\partial \lambda_{c,N+1}}\right|_{\lambda^p_{c,N+1}} - \left.\frac{\partial x_{1,N+1}}{\partial \lambda_{c,N+1}}\right|_{\lambda^p_{c,N+1}}\right) + \beta \cdot \left(\left.\frac{\partial v_{2,N+1}}{\partial \lambda_{c,N+1}}\right|_{\lambda^p_{c,N+1}} - \left.\frac{\partial v_{1,N+1}}{\partial \lambda_{c,N+1}}\right|_{\lambda^p_{c,N+1}}\right) + \cdots} \,. \tag{15}$$

**Step 3: Corrector step**

- Using the corrected coupling force $\lambda_{c,N+1}$ from Eq. (15), the integration of subsystem 1 and subsystem 2 from $T_N$ to $T_{N+1}$ with the initial conditions (5a) yields the corrected state variables

$$\begin{aligned} x_{1,N+1} &= x_{1,N+1}(\lambda_{c,N+1})\,, \qquad v_{1,N+1} = v_{1,N+1}(\lambda_{c,N+1})\,, \\ x_{2,N+1} &= x_{2,N+1}(\lambda_{c,N+1})\,, \qquad v_{2,N+1} = v_{2,N+1}(\lambda_{c,N+1})\,. \end{aligned} \tag{16}$$

#### 2.1.1 Semi-implicit index-3 co-simulation approach

For $\beta = \gamma = 0$, the semi-implicit co-simulation technique described above is a coupling approach on index-3 level. In this case, evaluation of Eq. (8) and Eq. (11) can be omitted. Furthermore, in Eq. (12) only the partial derivatives (a) and (d) have to be calculated.

#### 2.1.2 Semi-implicit index-2 co-simulation approach

Choosing $\beta > 0$ and $\gamma = 0$ yields a co-simulation approach on index-2 level. Applying the index-2 approach, evaluation of Eq. (8) and Eq. (11) is not required and in Eq. (12) the calculation of the partial derivatives (c) and (f) can be omitted.

#### 2.1.3 Semi-implicit index-1 co-simulation approach

Choosing $\beta > 0$ and $\gamma > 0$ yields an index-1 co-simulation approach.

### 2.2 Method 2: Semi-implicit co-simulation approach based on weighted multipliers

The second method is called weighted multiplier method within this manuscript and makes use of the coupling equations on position, velocity and acceleration level in order to calculate corrected coupling variables for the corrector step. Method 2 is very similar to method 1 discussed in Sect. 2.1; the methods only differ in the calculation of the corrected coupling force $\lambda_{c,N+1}$. The decomposed 1-DOF oscillator is now described by the following equations

Subsystem 1:

$$\dot{x}_1 = v_1\,, \qquad \dot{v}_1 = -\frac{c_1}{m_1}x_1 - \frac{d_1}{m_1}v_1 + \frac{\lambda_c}{m_1}\,, \tag{17a}$$

Subsystem 2:

$$\dot{x}_2 = v_2\,, \qquad \dot{v}_2 = -\frac{c_2}{m_2}x_2 - \frac{d_2}{m_2}v_2 - \frac{\lambda_c}{m_2}\,, \tag{17b}$$

Coupling conditions:

$$g_{c\lambda} := x_2 - x_1 = 0\,, \quad \dot{g}_{c\lambda} := v_2 - v_1 = 0\,, \quad \ddot{g}_{c\lambda} := \dot{v}_2 - \dot{v}_1 = 0\,. \tag{17c}$$

**Step 1: Predictor step**

- The predictor step is equivalent to method 1 in Sect. 2.1.

 

**Step 2: Calculation of corrected coupling force**

- Calculation of the partial derivatives according to Eq. (12) is also equivalent to method 1 in Sect. 2.1.
- For calculating the corrected (improved) coupling force $\lambda_{c,N+1}$, we consider the 3 coupling conditions (17c) at the fixed time point $T_{N+1}$ and interpret $g_{c\lambda,N+1}$, $\dot{g}_{c\lambda,N+1}$, and $\ddot{g}_{c\lambda,N+1}$ as functions of the coupling force $\lambda_{c,N+1}$

$$\begin{aligned} g_{c\lambda,N+1}(\lambda_{c,N+1}) &:= x_{2,N+1}(\lambda_{c,N+1}) - x_{1,N+1}(\lambda_{c,N+1})\,, \\ \dot{g}_{c\lambda,N+1}(\lambda_{c,N+1}) &:= v_{2,N+1}(\lambda_{c,N+1}) - v_{1,N+1}(\lambda_{c,N+1})\,, \\ \ddot{g}_{c\lambda,N+1}(\lambda_{c,N+1}) &:= \dot{v}_{2,N+1}(\lambda_{c,N+1}) - \dot{v}_{1,N+1}(\lambda_{c,N+1})\,. \end{aligned} \tag{18}$$

Next, the functions $g_{c\lambda,N+1}(\lambda_{c,N+1})$, $\dot{g}_{c\lambda,N+1}(\lambda_{c,N+1})$, and $\ddot{g}_{c\lambda,N+1}(\lambda_{c,N+1})$ are expanded in a Taylor series with respect to $\lambda_{c,N+1}$. As expansion point, we choose $\lambda^p_{c,N+1}$. Neglecting the higher order terms $\mathcal{O}(\lambda^2_{c,N+1})$, a Taylor series expansion of $g_{c\lambda,N+1}(\lambda_{c,N+1})$, $\dot{g}_{c\lambda,N+1}(\lambda_{c,N+1})$, and $\ddot{g}_{c\lambda,N+1}(\lambda_{c,N+1})$ yields the linearized coupling conditions

$$\begin{aligned} g^{linear}_{c\lambda,N+1}(\lambda_{c,N+1}) &:= g_{c\lambda,N+1}(\lambda^p_{c,N+1}) + \left.\frac{\partial g_{c\lambda,N+1}}{\partial \lambda_{c,N+1}}\right|_{\lambda^p_{c,N+1}} \cdot (\lambda_{c,N+1} - \lambda^p_{c,N+1}) \\ &= x_{2,N+1}(\lambda^p_{c,N+1}) - x_{1,N+1}(\lambda^p_{c,N+1}) \\ &\quad + \left( \left.\frac{\partial x_{2,N+1}}{\partial \lambda_{c,N+1}}\right|_{\lambda^p_{c,N+1}} - \left.\frac{\partial x_{1,N+1}}{\partial \lambda_{c,N+1}}\right|_{\lambda^p_{c,N+1}} \right) \cdot (\lambda_{c,N+1} - \lambda^p_{c,N+1}) = 0\,, \end{aligned} \tag{19a}$$

$$\begin{aligned} \dot{g}^{linear}_{c\lambda,N+1}(\lambda_{c,N+1}) &:= \dot{g}_{c\lambda,N+1}(\lambda^p_{c,N+1}) + \left.\frac{\partial \dot{g}_{c\lambda,N+1}}{\partial \lambda_{c,N+1}}\right|_{\lambda^p_{c,N+1}} \cdot (\lambda_{c,N+1} - \lambda^p_{c,N+1}) \\ &= v_{2,N+1}(\lambda^p_{c,N+1}) - v_{1,N+1}(\lambda^p_{c,N+1}) \\ &\quad + \left( \left.\frac{\partial v_{2,N+1}}{\partial \lambda_{c,N+1}}\right|_{\lambda^p_{c,N+1}} - \left.\frac{\partial v_{1,N+1}}{\partial \lambda_{c,N+1}}\right|_{\lambda^p_{c,N+1}} \right) \cdot (\lambda_{c,N+1} - \lambda^p_{c,N+1}) = 0\,, \end{aligned} \tag{19b}$$

$$\begin{aligned} \ddot{g}^{linear}_{c\lambda,N+1}(\lambda_{c,N+1}) &:= \ddot{g}_{c\lambda,N+1}(\lambda^p_{c,N+1}) + \left.\frac{\partial \ddot{g}_{c\lambda,N+1}}{\partial \lambda_{c,N+1}}\right|_{\lambda^p_{c,N+1}} \cdot (\lambda_{c,N+1} - \lambda^p_{c,N+1}) \\ &= \dot{v}_{2,N+1}(\lambda^p_{c,N+1}) - \dot{v}_{1,N+1}(\lambda^p_{c,N+1}) \\ &\quad + \left( \left.\frac{\partial \dot{v}_{2,N+1}}{\partial \lambda_{c,N+1}}\right|_{\lambda^p_{c,N+1}} - \left.\frac{\partial \dot{v}_{1,N+1}}{\partial \lambda_{c,N+1}}\right|_{\lambda^p_{c,N+1}} \right) \cdot (\lambda_{c,N+1} - \lambda^p_{c,N+1}) = 0\,. \end{aligned} \tag{19c}$$

- Solving the linearized coupling condition (19a) for the coupling force yields the corrected Lagrange multiplier

$$\lambda^{pos}_{c,N+1} = \lambda^p_{c,N+1} - \frac{x_{2,N+1}(\lambda^p_{c,N+1}) - x_{1,N+1}(\lambda^p_{c,N+1})}{\left.\frac{\partial x_{2,N+1}}{\partial \lambda_{c,N+1}}\right|_{\lambda^p_{c,N+1}} - \left.\frac{\partial x_{1,N+1}}{\partial \lambda_{c,N+1}}\right|_{\lambda^p_{c,N+1}}}\,. \tag{20}$$

Solving the linearized coupling condition (19b) for the coupling force yields the corrected Lagrange multiplier

$$\lambda^{vel}_{c,N+1} = \lambda^p_{c,N+1} - \frac{v_{2,N+1}(\lambda^p_{c,N+1}) - v_{1,N+1}(\lambda^p_{c,N+1})}{\left.\frac{\partial v_{2,N+1}}{\partial \lambda_{c,N+1}}\right|_{\lambda^p_{c,N+1}} - \left.\frac{\partial v_{1,N+1}}{\partial \lambda_{c,N+1}}\right|_{\lambda^p_{c,N+1}}}\,. \tag{21}$$

Solving the linearized coupling condition (19c) for the coupling force yields the corrected Lagrange multiplier

$$\lambda^{acc}_{c,N+1} = \lambda^p_{c,N+1} - \frac{\dot{v}_{2,N+1}(\lambda^p_{c,N+1}) - \dot{v}_{1,N+1}(\lambda^p_{c,N+1})}{\left.\frac{\partial \dot{v}_{2,N+1}}{\partial \lambda_{c,N+1}}\right|_{\lambda^p_{c,N+1}} - \left.\frac{\partial \dot{v}_{1,N+1}}{\partial \lambda_{c,N+1}}\right|_{\lambda^p_{c,N+1}}}\,. \tag{22}$$

- Within the weighted multiplier method, the corrected coupling force is calculated by

$$\lambda_{c,N+1} = \frac{1}{1+a+b}\left(\lambda^{pos}_{c,N+1} + a\cdot\lambda^{vel}_{c,N+1} + b\cdot\lambda^{acc}_{c,N+1}\right), \tag{23}$$

  where $a \geq 0$ and $b \geq 0$ are real-valued user-defined parameters (e.g. $a = b = 1$).

**Step 3: Corrector step**

- The corrector step is equivalent to method 1 in Sect. 2.1 with the only difference that $\lambda_{c,N+1}$ from Eq. (23) is used instead of $\lambda_{c,N+1}$ from Eq. (15).

#### 2.2.1 Semi-implicit index-3 co-simulation approach

For $a = b = 0$, method 2 is equivalent to the index-3 formulation of method 1, see Sect. 2.1.1.

#### 2.2.2 Semi-implicit index-2 co-simulation approach

Choosing $a > 0$ and $b = 0$ results in a co-simulation approach on index-2 level. In this case, evaluation of Eq. (8) and Eq. (11) is not necessary and the partial derivatives (c) and (f) in Eq. (12) are not required.

#### 2.2.3 Semi-implicit index-1 co-simulation approach

Choosing $a > 0$ and $b > 0$ yields an index-1 co-simulation approach.

### 2.3 Remark on the difference between method 1 and method 2

The two presented methods are obviously closely related, since both methods use the same ingredients – namely the same predicted variables and the same partial derivatives – for calculating corrected coupling variables. The difference of the two approaches lies in the combination of these ingredients. Hence, the two methods are not identical and in general yield different results. By simply comparing Eq. (15) with Eq. (23) (or the general expressions (68) and (76) in Sect. 3), it can easily be seen that running a co-simulation with a constant set of Baumgarte parameters $\beta$ and $\gamma$ corresponds to a simulation with varying parameters $a$ and $b$. Assume for instance that a macro-time step has been accomplished with the Baumgarte parameters $\beta$ and $\gamma$, i.e. with the corrected coupling variable $\lambda_{c,N+1}$ according to Eq. (15). The same corrected coupling variable $\lambda_{c,N+1}$ and therefore the same corrected state variables can be achieved with the weighted multiplier method based on Eq. (23). Specifying $\beta$ and $\gamma$, corresponding parameters $a$ and $b$ can simply be calculated by combining Eq. (15) and Eq. (23), i.e. by using the relationship

$$\begin{aligned}\lambda^{p}_{c,N+1} - \frac{\left(x_{2,N+1}(\lambda^{p}_{c,N+1}) - x_{1,N+1}(\lambda^{p}_{c,N+1})\right) + \beta\cdot\left(v_{2,N+1}(\lambda^{p}_{c,N+1}) - v_{1,N+1}(\lambda^{p}_{c,N+1})\right) + \cdots}{\left(\left.\frac{\partial x_{2,N+1}}{\partial\lambda_{c,N+1}}\right|_{\lambda^{p}_{c,N+1}} - \left.\frac{\partial x_{1,N+1}}{\partial\lambda_{c,N+1}}\right|_{\lambda^{p}_{c,N+1}}\right) + \beta\cdot\left(\left.\frac{\partial v_{2,N+1}}{\partial\lambda_{c,N+1}}\right|_{\lambda^{p}_{c,N+1}} - \left.\frac{\partial v_{1,N+1}}{\partial\lambda_{c,N+1}}\right|_{\lambda^{p}_{c,N+1}}\right) + \cdots} \\ = \frac{1}{1+a+b}\left(\lambda^{pos}_{c,N+1} + a\cdot\lambda^{vel}_{c,N+1} + b\cdot\lambda^{acc}_{c,N+1}\right).\end{aligned} \tag{24}$$

As can be seen, $a$ and $b$ are not uniquely determined so that different combinations of $a$ and $b$ may yield the same $\lambda_{c,N+1}$ (specified by $\beta$ and $\gamma$). Since the predicted variables and the partial derivatives usually change in each macro-time step, a set of constant Baumgarte parameters $\beta$ and $\gamma$ corresponds to a varying set of parameters $a$ and $b$. Consequently, simulation results calculated with constant parameters $\beta$ and $\gamma$ cannot be reproduced by a co-simulation with constant parameters $a$ and $b$.

## 3 Semi-implicit co-simulation approaches for general mechanical systems

### 3.1 Definition of the 2 coupled mechanical subsystems

In this section, the semi-implicit approaches are generalized and applied to couple 2 arbitrary mechanical subsystems. Concretely, subsystem 1 is a mechanical system consisting of $n_1$ rigid bodies. Subsystem 2 collects $n_2$ rigid bodies. Both subsystems are assumed to be general multibody systems, mathematically described by 2 DAE systems. The subsystems

 

are mechanically coupled by algebraic constraint equations. More precisely, marker $K_{C_i}$ of body $i$ belonging to subsystem 1 is connected to marker $K_{C_j}$ of body $j$ belonging to subsystem 2 by a rigid joint, see Fig. 3. In Fig. 3, the inertial reference frame is denoted by $K_0$. $S_i$ terms the center of mass of body $i$ and $\boldsymbol{r}_{S_i}$ represents the position vector to $S_i$. At the center of mass, the body fixed principal axes system $K_{S_i}$ is defined. To describe the coupling point $C_i$, the body fixed vector $\boldsymbol{r}_{C_i}$ is used. At $C_i$, the body fixed system $K_{C_i}$ is attached, which is assumed to be parallel to $K_{S_i}$. The notation for subsystem 2 is equivalent $(i \to j)$.

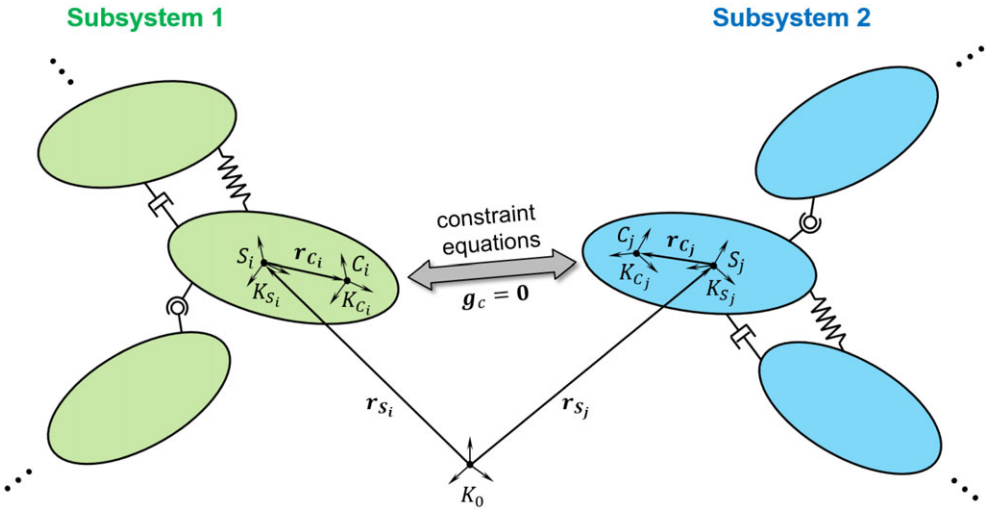


**Fig. 3** Body $i$ of subsystem 1 coupled to body $j$ of subsystem 2 by algebraic constraint equations (coupling points $C_i$ and $C_j$).

Let $\boldsymbol{a} \in \mathbb{R}^3$ term an arbitrary vector. Its coordinates with respect to system $K_m$ are denoted by ${}^m\boldsymbol{a}$. By means of the transformation matrix ${}^{nm}\boldsymbol{T} \in \mathbb{R}^{3\times3}$, the vector coordinates can be transformed from system $K_m$ to system $K_n$ using the relationship ${}^n\boldsymbol{a} = {}^{nm}\boldsymbol{T}\,{}^m\boldsymbol{a}$.

Within this paper, absolute coordinates are used to describe multibody systems [17]. Hence, the translation of an arbitrary rigid body $q$ is described by the 3 coordinates of the center of mass ${}^0\boldsymbol{r}_{S_q}$. The orientation of the body is defined by 3 rotation parameters $\boldsymbol{\gamma}_q \in \mathbb{R}^3$ (e.g. by 3 Euler angles). The velocity of the center of mass $S_q$ is calculated by the time derivative of the position vector ${}^0\boldsymbol{v}_{S_q} = {}^0\dot{\boldsymbol{r}}_{S_q}$. The coordinates of the angular velocity with respect to the body fixed system $K_{S_q}$ is related to the time derivative of the rotation parameters by the general expression $\dot{\boldsymbol{\gamma}}_q = \boldsymbol{B}(\boldsymbol{\gamma}_q)\,{}^q\boldsymbol{\omega}_q$. If Euler angles are used as rotation parameters, i.e. $\boldsymbol{\gamma}_q = (\psi_q \;\; \phi_q \;\; \theta_q)^T$, the matrix $\boldsymbol{B}(\boldsymbol{\gamma}_q) \in \mathbb{R}^{3\times3}$ is found to be

$$\boldsymbol{B} = \frac{1}{\sin\theta_q}\begin{pmatrix} \sin\phi_q & \cos\phi_q & 0 \\ \sin\theta_q\cos\phi_q & -\sin\theta_q\sin\phi_q & 0 \\ -\cos\theta_q\sin\phi_q & -\cos\theta_q\cos\phi_q & \sin\theta_q \end{pmatrix}. \tag{25}$$

For the following analysis, it is useful to define some auxiliary vectors. The vector $\boldsymbol{z}_i = (z_{i1} \;\; z_{i2} \;\; \cdots \;\; z_{i12})^T = ({}^0\boldsymbol{r}_{S_i} \;\; \boldsymbol{\gamma}_i \;\; {}^0\boldsymbol{v}_{S_i} \;\; {}^i\boldsymbol{\omega}_i)^T \in \mathbb{R}^{12}$ and the vector $\boldsymbol{z}_j = (z_{j1} \;\; z_{j2} \;\; \cdots \;\; z_{j12})^T = ({}^0\boldsymbol{r}_{S_j} \;\; \boldsymbol{\gamma}_j \;\; {}^0\boldsymbol{v}_{S_j} \;\; {}^j\boldsymbol{\omega}_j)^T \in \mathbb{R}^{12}$ contain the position and velocity coordinates of the coupling bodies $i$ and $j$. The position and velocity coordinates of both coupling bodies are collected in the vector $\boldsymbol{z}_c = (\boldsymbol{z}_i \;\; \boldsymbol{z}_j)^T \in \mathbb{R}^{24}$. Furthermore, the vector $\hat{\boldsymbol{z}}_1 \in \mathbb{R}^{12\cdot n_1}$ contains the position and velocity coordinates of all bodies of subsystem 1 and the vector $\hat{\boldsymbol{z}}_2 \in \mathbb{R}^{12\cdot n_2}$ the position and velocity coordinates of all bodies of subsystem 2. The vector $\boldsymbol{a}_i = (a_{i1} \;\; a_{i2} \;\; \cdots \;\; a_{i6})^T = \left({}^0\dot{\boldsymbol{v}}_{S_i} \;\; {}^i\dot{\boldsymbol{\omega}}_i\right)^T \in \mathbb{R}^6$ collects the accelerations of the coupling body $i$ and the vector $\boldsymbol{a}_j = (a_{j1} \;\; a_{j2} \;\; \cdots \;\; a_{j6})^T = \left({}^0\dot{\boldsymbol{v}}_{S_j} \;\; {}^j\dot{\boldsymbol{\omega}}_j\right)^T \in \mathbb{R}^6$ the corresponding accelerations of the coupling body $j$. The accelerations of both coupling bodies are combined in the vector $\boldsymbol{a}_c = (\boldsymbol{a}_i \;\; \boldsymbol{a}_j)^T \in \mathbb{R}^{12}$.

Next, the equations of motion for the coupling bodies $i$ and $j$ are derived. Therefore, we formulate Newton's law with respect to $K_0$ for both bodies and Euler's law with respect to the body fixed system $K_{S_i}$ and $K_{S_j}$, respectively. This yields

Coupling body $i$ (subsystem 1):

$$\begin{aligned} &{}^0\dot{\boldsymbol{r}}_{S_i} = {}^0\boldsymbol{v}_{S_i}\,, \qquad m_i\,{}^0\dot{\boldsymbol{v}}_{S_i} = {}^0\boldsymbol{F}_{a_i}(\hat{\boldsymbol{z}}_1, t) + {}^0\boldsymbol{F}_{r_i} + {}^0\boldsymbol{F}_{c_i}(\boldsymbol{z}_c)\,, \\ &\dot{\boldsymbol{\gamma}}_i = \boldsymbol{B}(\boldsymbol{\gamma}_i)\,{}^i\boldsymbol{\omega}_i\,, \quad {}^i\boldsymbol{J}_i\,{}^i\dot{\boldsymbol{\omega}}_i + {}^i\boldsymbol{\omega}_i \times {}^i\boldsymbol{J}_i\,{}^i\boldsymbol{\omega}_i = {}^i\boldsymbol{M}_{a_i}(\hat{\boldsymbol{z}}_1, t) + {}^i\boldsymbol{M}_{r_i} + {}^i\boldsymbol{M}_{c_i}(\boldsymbol{z}_c)\,. \end{aligned} \tag{26}$$

Coupling body $j$ (subsystem 2):

$$
\begin{aligned}
&{}^0\dot{\boldsymbol{r}}_{S_j} = {}^0\boldsymbol{v}_{S_j}\,, \qquad m_j\,{}^0\dot{\boldsymbol{v}}_{S_j} = {}^0\boldsymbol{F}_{a_j}(\hat{\boldsymbol{z}}_2,t) + {}^0\boldsymbol{F}_{r_j} + {}^0\boldsymbol{F}_{c_j}(\boldsymbol{z}_c)\,,\\
&\dot{\boldsymbol{\gamma}}_j = \boldsymbol{B}(\boldsymbol{\gamma}_j)\,{}^j\boldsymbol{\omega}_j\,, \quad {}^j\boldsymbol{J}_j\,{}^j\dot{\boldsymbol{\omega}}_j + {}^j\boldsymbol{\omega}_j \times {}^j\boldsymbol{J}_j\,{}^j\boldsymbol{\omega}_j = {}^j\boldsymbol{M}_{a_j}(\hat{\boldsymbol{z}}_2,t) + {}^j\boldsymbol{M}_{r_j} + {}^j\boldsymbol{M}_{c_j}(\boldsymbol{z}_c)\,.
\end{aligned}
\tag{27}
$$

In the above equations, $m_i$ represents the mass of the coupling body $i$ and ${}^i\boldsymbol{J}_i$ the coordinates of the inertia tensor with respect to $K_{S_i}$. ${}^0\boldsymbol{F}_{a_i}$ denotes the vector of externally applied forces (represented in $K_0$) and ${}^i\boldsymbol{M}_{a_i}$ the vector of externally applied torques (represented in $K_{S_i}$). ${}^0\boldsymbol{F}_{r_i}$ and ${}^i\boldsymbol{M}_{r_i}$ term the reaction forces and torques resulting from algebraic constraints in subsystem 1. ${}^0\boldsymbol{F}_{c_i}$ and ${}^i\boldsymbol{M}_{c_i}$ are the coupling forces and coupling torques, generated by the algebraic coupling constraints. An equivalent notation is used for the coupling body $j$.

### 3.2 Coupling of subsystems: Concept of fundamental joints

In the following, we describe in detail the coupling forces/torques as well as the coupling conditions for 3 fundamental joints, namely for the *atpoint joint*, for the *inplane joint* and for the *perpendicular joint*. Combining different fundamental joints, other joints can be generated [17], e.g.

- the *universal joint* (1 atpoint joint + 1 perpendicular joint),
- the *revolute joint* (1 atpoint joint + 2 perpendicular joints),
- the *translational joint* (3 perpendicular joints + 2 inplane joints),
- the *cylindrical joint* (2 perpendicular joints + 2 inplane joints),
- the *planar joint* (2 perpendicular joints + 1 inplane joint),
- the *inline joint* (2 inplane joints) and
- the *orientation joint* (3 perpendicular joints).

#### 3.2.1 Atpoint joint (spherical joint)

The first fundamental joint is the *atpoint joint*, described by the constraint condition

$$
(\boldsymbol{r}_{S_i} + \boldsymbol{r}_{C_i}) - \left(\boldsymbol{r}_{S_j} + \boldsymbol{r}_{C_j}\right) = \boldsymbol{0}\,. \tag{28}
$$

This constraint enforces that the coupling points $C_i$ and $C_j$ coincide. Decomposing the vectors in Eq. (28) with respect to $K_0$ and collecting the 3 scalar constraint equations in the constraint vector $\boldsymbol{g}_{ca} \in \mathbb{R}^3$ yields

$$
\boldsymbol{g}_{ca} := \left({}^0\boldsymbol{r}_{S_i} + {}^{0i}\boldsymbol{T}(\boldsymbol{\gamma}_i)\,{}^i\boldsymbol{r}_{C_i}\right) - \left({}^0\boldsymbol{r}_{S_j} + {}^{0j}\boldsymbol{T}(\boldsymbol{\gamma}_j)\,{}^j\boldsymbol{r}_{C_j}\right) = \boldsymbol{0}\,. \tag{29}
$$

The 3 constraint equations (29) generate the following constraint forces and constraint torques (see Eqs. (26) and (27))

$$
\begin{aligned}
&{}^0\boldsymbol{F}_{c_i} = {}^0\boldsymbol{\lambda}_{ca}\,, \qquad {}^i\boldsymbol{M}_{c_i} = {}^i\boldsymbol{r}_{C_i} \times {}^{i0}\boldsymbol{T}(\boldsymbol{\gamma}_i)\,{}^0\boldsymbol{\lambda}_{ca}\,,\\
&{}^0\boldsymbol{F}_{c_j} = -{}^0\boldsymbol{\lambda}_{ca}\,, \quad {}^j\boldsymbol{M}_{c_j} = -{}^j\boldsymbol{r}_{C_j} \times {}^{j0}\boldsymbol{T}(\boldsymbol{\gamma}_j)\,{}^0\boldsymbol{\lambda}_{ca}\,,
\end{aligned}
\tag{30}
$$

where ${}^0\boldsymbol{\lambda}_{ca} = ({}^0\lambda_{ca_x}\ {}^0\lambda_{ca_y}\ {}^0\lambda_{ca_z})^T$ collects the 3 Lagrange multipliers.

**Semi-implicit co-simulation approach based on Baumgarte-stabilization:**
Using the Baumgarte-stabilization approach, the constraint equation (28) is replaced by the coupling condition

$$
\begin{aligned}
&\left[(\boldsymbol{r}_{S_i} + \boldsymbol{r}_{C_i}) - \left(\boldsymbol{r}_{S_j} + \boldsymbol{r}_{C_j}\right)\right] + \beta \cdot \frac{d}{dt}\left\{\left[(\boldsymbol{r}_{S_i} + \boldsymbol{r}_{C_i}) - \left(\boldsymbol{r}_{S_j} + \boldsymbol{r}_{C_j}\right)\right]\right\}\\
&+ \gamma \cdot \frac{d^2}{dt^2}\left\{\left[(\boldsymbol{r}_{S_i} + \boldsymbol{r}_{C_i}) - \left(\boldsymbol{r}_{S_j} + \boldsymbol{r}_{C_j}\right)\right]\right\} = \boldsymbol{0}\,.
\end{aligned}
\tag{31}
$$

Note that $\dfrac{d}{dt}$ terms the total time derivative, i.e. the time derivative with respect to $K_0$. Representing the vectors in Eq. (31) with respect to the system $K_0$ and formally collecting the 3 scalar coupling conditions in the vector $\boldsymbol{g}_{ca}^B \in \mathbb{R}^3$ yields

$$
\begin{aligned}
\boldsymbol{g}_{ca}^B := &\left[\left({}^0\boldsymbol{r}_{S_i} + {}^{0i}\boldsymbol{T}(\boldsymbol{\gamma}_i)\,{}^i\boldsymbol{r}_{C_i}\right) - \left({}^0\boldsymbol{r}_{S_j} + {}^{0j}\boldsymbol{T}(\boldsymbol{\gamma}_j)\,{}^j\boldsymbol{r}_{C_j}\right)\right]\\
&+ \beta \cdot \left[\left({}^0\boldsymbol{v}_{S_i} + {}^{0i}\boldsymbol{T}(\boldsymbol{\gamma}_i)\,{}^i\boldsymbol{\omega}_i \times {}^{0i}\boldsymbol{T}(\boldsymbol{\gamma}_i)\,{}^i\boldsymbol{r}_{C_i}\right) - \left({}^0\boldsymbol{v}_{S_j} + {}^{0j}\boldsymbol{T}(\boldsymbol{\gamma}_j)\,{}^j\boldsymbol{\omega}_j \times {}^{0j}\boldsymbol{T}(\boldsymbol{\gamma}_j)\,{}^j\boldsymbol{r}_{C_j}\right)\right]\\
&+ \gamma \cdot \frac{d}{dt}\left[\left({}^0\boldsymbol{v}_{S_i} + {}^{0i}\boldsymbol{T}(\boldsymbol{\gamma}_i)\,{}^i\boldsymbol{\omega}_i \times {}^{0i}\boldsymbol{T}(\boldsymbol{\gamma}_i)\,{}^i\boldsymbol{r}_{C_i}\right) - \left({}^0\boldsymbol{v}_{S_j} + {}^{0j}\boldsymbol{T}(\boldsymbol{\gamma}_j)\,{}^j\boldsymbol{\omega}_j \times {}^{0j}\boldsymbol{T}(\boldsymbol{\gamma}_j)\,{}^j\boldsymbol{r}_{C_j}\right)\right] = \boldsymbol{0}\,.
\end{aligned}
\tag{32}
$$

 

For the reason of a concise representation, the second time derivative is not carried out explicitly.

Hence, connecting $C_i$ and $C_j$ by an atpoint joint and applying the Baumgarte-stabilization approach, the coupling forces/ torques and the 3 scalar coupling conditions read as

$$
\begin{aligned}
&{}^0\boldsymbol{F}_{c_i} = {}^0\boldsymbol{\lambda}_{ca}\,, \qquad {}^i\boldsymbol{M}_{c_i} = {}^i\boldsymbol{r}_{C_i} \times {}^{i0}\boldsymbol{T}(\boldsymbol{\gamma}_i)\,{}^0\boldsymbol{\lambda}_{ca}\,,\\
&{}^0\boldsymbol{F}_{c_j} = -{}^0\boldsymbol{\lambda}_{ca}\,, \quad {}^j\boldsymbol{M}_{c_j} = -{}^j\boldsymbol{r}_{C_j} \times {}^{j0}\boldsymbol{T}(\boldsymbol{\gamma}_j)\,{}^0\boldsymbol{\lambda}_{ca}\,,\\
&\boldsymbol{g}_{ca}^B = \boldsymbol{0}\,.
\end{aligned}
\tag{33}
$$

According to the nomenclature in Sect. 3.3.1, the input vectors for the coupling bodies $i$ and $j$ are given by $\tilde{\boldsymbol{u}}_j = {}^0\boldsymbol{\lambda}_{ca} \in \mathbb{R}^3$ and $\tilde{\boldsymbol{u}}_i = {}^0\boldsymbol{\lambda}_{ca} \in \mathbb{R}^3$. The vector collecting the coupling equations is given by $\boldsymbol{g}_c^B = \boldsymbol{g}_{ca}^B \in \mathbb{R}^3$.

**Semi-implicit co-simulation approach based on weighted multipliers:**

For the weighted multiplier co-simulation method, the constraint equation (28) is complemented by the coupling conditions on velocity and on acceleration level

$$
\begin{aligned}
&(\boldsymbol{r}_{S_i} + \boldsymbol{r}_{C_i}) - \left(\boldsymbol{r}_{S_j} + \boldsymbol{r}_{C_j}\right) = \boldsymbol{0}\,,\\
&\frac{d}{dt}\left\{(\boldsymbol{r}_{S_i} + \boldsymbol{r}_{C_i}) - \left(\boldsymbol{r}_{S_j} + \boldsymbol{r}_{C_j}\right)\right\} = \boldsymbol{0}\,,\\
&\frac{d^2}{dt^2}\left\{(\boldsymbol{r}_{S_i} + \boldsymbol{r}_{C_i}) - \left(\boldsymbol{r}_{S_j} + \boldsymbol{r}_{C_j}\right)\right\} = \boldsymbol{0}\,.
\end{aligned}
\tag{34}
$$

Representing the vectors of Eq. (34) with respect to the system $K_0$ and formally collecting the scalar coupling conditions in the vectors $\boldsymbol{g}_{ca}, \dot{\boldsymbol{g}}_{ca}, \ddot{\boldsymbol{g}}_{ca} \in \mathbb{R}^3$ yields

$$
\begin{aligned}
&\boldsymbol{g}_{ca} := \left({}^0\boldsymbol{r}_{S_i} + {}^{0i}\boldsymbol{T}(\boldsymbol{\gamma}_i)\,{}^i\boldsymbol{r}_{C_i}\right) - \left({}^0\boldsymbol{r}_{S_j} + {}^{0j}\boldsymbol{T}(\boldsymbol{\gamma}_j)\,{}^j\boldsymbol{r}_{C_j}\right) = \boldsymbol{0}\,,\\
&\dot{\boldsymbol{g}}_{ca} := \left({}^0\boldsymbol{v}_{S_i} + {}^{0i}\boldsymbol{T}(\boldsymbol{\gamma}_i)\,{}^i\boldsymbol{\omega}_i \times {}^{0i}\boldsymbol{T}(\boldsymbol{\gamma}_i)\,{}^i\boldsymbol{r}_{C_i}\right) - \left({}^0\boldsymbol{v}_{S_j} + {}^{0j}\boldsymbol{T}(\boldsymbol{\gamma}_j)\,{}^j\boldsymbol{\omega}_j \times {}^{0j}\boldsymbol{T}(\boldsymbol{\gamma}_j)\,{}^j\boldsymbol{r}_{C_j}\right) = \boldsymbol{0}\,,\\
&\ddot{\boldsymbol{g}}_{ca} := \frac{d}{dt}\left\{\left({}^0\boldsymbol{v}_{S_i} + {}^{0i}\boldsymbol{T}(\boldsymbol{\gamma}_i)\,{}^i\boldsymbol{\omega}_i \times {}^{0i}\boldsymbol{T}(\boldsymbol{\gamma}_i)\,{}^i\boldsymbol{r}_{C_i}\right) - \left({}^0\boldsymbol{v}_{S_j} + {}^{0j}\boldsymbol{T}(\boldsymbol{\gamma}_j)\,{}^j\boldsymbol{\omega}_j \times {}^{0j}\boldsymbol{T}(\boldsymbol{\gamma}_j)\,{}^j\boldsymbol{r}_{C_j}\right)\right\} = \boldsymbol{0}\,.
\end{aligned}
\tag{35}
$$

Connecting $C_i$ and $C_j$ by an atpoint joint and applying the weighted multiplier co-simulation approach, the coupling forces/torques and the 9 scalar coupling conditions are defined by

$$
\begin{aligned}
&{}^0\boldsymbol{F}_{c_i} = {}^0\boldsymbol{\lambda}_{ca}\,, \qquad {}^i\boldsymbol{M}_{c_i} = {}^i\boldsymbol{r}_{C_i} \times {}^{i0}\boldsymbol{T}(\boldsymbol{\gamma}_i)\,{}^0\boldsymbol{\lambda}_{ca}\,,\\
&{}^0\boldsymbol{F}_{c_j} = -{}^0\boldsymbol{\lambda}_{ca}\,, \quad {}^j\boldsymbol{M}_{c_j} = -{}^j\boldsymbol{r}_{C_j} \times {}^{j0}\boldsymbol{T}(\boldsymbol{\gamma}_j)\,{}^0\boldsymbol{\lambda}_{ca}\,,\\
&\boldsymbol{g}_{ca} = \boldsymbol{0}\,,\ \dot{\boldsymbol{g}}_{ca} = \boldsymbol{0}\,,\ \ddot{\boldsymbol{g}}_{ca} = \boldsymbol{0}\,.
\end{aligned}
\tag{36}
$$

According to the nomenclature in Sect. 3.3.2, the input vectors for the coupling bodies $i$ and $j$ are given by $\tilde{\boldsymbol{u}}_j = {}^0\boldsymbol{\lambda}_{ca} \in \mathbb{R}^3$ and $\tilde{\boldsymbol{u}}_i = {}^0\boldsymbol{\lambda}_{ca} \in \mathbb{R}^3$. The 3 vectors collecting the coupling equations are given by $\boldsymbol{g}_c^{pos} = \boldsymbol{g}_{ca}$, $\boldsymbol{g}_c^{vel} = \dot{\boldsymbol{g}}_{ca}$, $\boldsymbol{g}_c^{acc} = \ddot{\boldsymbol{g}}_{ca} \in \mathbb{R}^3$.

### 3.2.2 Inplane joint

The second fundamental joint is the *inplane joint*, described by the scalar constraint equation

$$
\left[(\boldsymbol{r}_{S_i} + \boldsymbol{r}_{C_i}) - \left(\boldsymbol{r}_{S_j} + \boldsymbol{r}_{C_j}\right)\right] \cdot \boldsymbol{e}_j = 0\,,
\tag{37}
$$

where $\boldsymbol{e}_j$ denotes an arbitrary unit vector fixed at body $j$. The constraint equation (37) enforces that the point $C_i$ remains in the plane with normal vector $\boldsymbol{e}_j$ fixed at point $C_j$. Decomposition with respect to the system $K_0$ yields

$$
g_{cd} := \left[\left({}^0\boldsymbol{r}_{S_i} + {}^{0i}\boldsymbol{T}(\boldsymbol{\gamma}_i)\,{}^i\boldsymbol{r}_{C_i}\right) - \left({}^0\boldsymbol{r}_{S_j} + {}^{0j}\boldsymbol{T}(\boldsymbol{\gamma}_j)\,{}^j\boldsymbol{r}_{C_j}\right)\right] \cdot {}^{0j}\boldsymbol{T}(\boldsymbol{\gamma}_j)\,{}^j\boldsymbol{e}_j = 0\,.
\tag{38}
$$

The constraint equation (38) entails the following constraint forces and constraint torques

$$
\begin{aligned}
&{}^0\boldsymbol{F}_{c_i} = {}^{0j}\boldsymbol{T}(\boldsymbol{\gamma}_j)\,{}^j\boldsymbol{e}_j\,\lambda_{cd}\,, \qquad {}^i\boldsymbol{M}_{c_i} = {}^i\boldsymbol{r}_{C_i} \times {}^{ij}\boldsymbol{T}(\boldsymbol{\gamma}_i, \boldsymbol{\gamma}_j)\,{}^j\boldsymbol{e}_j\,\lambda_{cd}\,,\\
&{}^0\boldsymbol{F}_{c_j} = -{}^{0j}\boldsymbol{T}(\boldsymbol{\gamma}_j)\,{}^j\boldsymbol{e}_j\,\lambda_{cd}\,, \quad {}^j\boldsymbol{M}_{c_j} = {}^j\boldsymbol{e}_j \times {}^{j0}\boldsymbol{T}(\boldsymbol{\gamma}_j)\left({}^0\boldsymbol{r}_{S_i} + {}^{0i}\boldsymbol{T}(\boldsymbol{\gamma}_i)\,{}^i\boldsymbol{r}_{C_i} - {}^0\boldsymbol{r}_{S_j}\right)\lambda_{cd}\,,
\end{aligned}
\tag{39}
$$

where $\lambda_{cd}$ terms the Lagrange multiplier.

**Semi-implicit co-simulation approach based on Baumgarte-stabilization:**
Using the Baumgarte-stabilization approach, the constraint equation (37) is replaced by the coupling condition

$$\begin{aligned}&\left[(\boldsymbol{r}_{S_i}+\boldsymbol{r}_{C_i})-\left(\boldsymbol{r}_{S_j}+\boldsymbol{r}_{C_j}\right)\right]\cdot\boldsymbol{e}_j+\beta\cdot\frac{d}{dt}\left\{\left[(\boldsymbol{r}_{S_i}+\boldsymbol{r}_{C_i})-\left(\boldsymbol{r}_{S_j}+\boldsymbol{r}_{C_j}\right)\right]\cdot\boldsymbol{e}_j\right\}\\&+\gamma\cdot\frac{d^2}{dt^2}\left\{\left[(\boldsymbol{r}_{S_i}+\boldsymbol{r}_{C_i})-\left(\boldsymbol{r}_{S_j}+\boldsymbol{r}_{C_j}\right)\right]\cdot\boldsymbol{e}_j\right\}=0\,.\end{aligned}\tag{40}$$

For the reason of a concise representation, the first and second time derivative of the constraint equation are not carried out explicitly. Evaluation of Eq. (40) with respect to the system $K_0$ yields

$$\begin{aligned}g_{cd}^B:=&\left[\left({}^0\boldsymbol{r}_{S_i}+{}^{0i}\boldsymbol{T}(\boldsymbol{\gamma}_i)^i\boldsymbol{r}_{C_i}\right)-\left({}^0\boldsymbol{r}_{S_j}+{}^{0j}\boldsymbol{T}(\boldsymbol{\gamma}_j)^j\boldsymbol{r}_{C_j}\right)\right]\cdot{}^{0j}\boldsymbol{T}(\boldsymbol{\gamma}_j)^j\boldsymbol{e}_j\\&+\beta\cdot\frac{d}{dt}\left\{\left[\left({}^0\boldsymbol{r}_{S_i}+{}^{0i}\boldsymbol{T}(\boldsymbol{\gamma}_i)^i\boldsymbol{r}_{C_i}\right)-\left({}^0\boldsymbol{r}_{S_j}+{}^{0j}\boldsymbol{T}(\boldsymbol{\gamma}_j)^j\boldsymbol{r}_{C_j}\right)\right]\cdot{}^{0j}\boldsymbol{T}(\boldsymbol{\gamma}_j)^j\boldsymbol{e}_j\right\}\\&+\gamma\cdot\frac{d^2}{dt^2}\left\{\left[\left({}^0\boldsymbol{r}_{S_i}+{}^{0i}\boldsymbol{T}(\boldsymbol{\gamma}_i)^i\boldsymbol{r}_{C_i}\right)-\left({}^0\boldsymbol{r}_{S_j}+{}^{0j}\boldsymbol{T}(\boldsymbol{\gamma}_j)^j\boldsymbol{r}_{C_j}\right)\right]\cdot{}^{0j}\boldsymbol{T}(\boldsymbol{\gamma}_j)^j\boldsymbol{e}_j\right\}=0\,.\end{aligned}\tag{41}$$

Connecting $C_i$ and $C_j$ by an inplane joint and applying the Baumgarte-stabilization approach, the coupling forces/torques and the 10 scalar coupling conditions read as

$$\begin{aligned}&{}^0\boldsymbol{F}_{c_i}={}^{0j}\boldsymbol{T}(\tilde{\boldsymbol{\gamma}}_j)\,{}^j\boldsymbol{e}_j\,\lambda_{cd}\,,\qquad{}^i\boldsymbol{M}_{c_i}={}^i\boldsymbol{r}_{C_i}\times{}^{ij}\boldsymbol{T}(\boldsymbol{\gamma}_i,\tilde{\boldsymbol{\gamma}}_j)\,{}^j\boldsymbol{e}_j\,\lambda_{cd}\,,\\&{}^0\boldsymbol{F}_{c_j}=-{}^{0j}\boldsymbol{T}(\boldsymbol{\gamma}_j)^j\boldsymbol{e}_j\,\lambda_{cd}\,,\qquad{}^j\boldsymbol{M}_{c_j}={}^j\boldsymbol{e}_j\times{}^{j0}\boldsymbol{T}(\boldsymbol{\gamma}_j)\left({}^0\tilde{\boldsymbol{r}}_{S_i}+{}^{0i}\boldsymbol{T}(\tilde{\boldsymbol{\gamma}}_i)\,{}^i\boldsymbol{r}_{C_i}-{}^0\boldsymbol{r}_{S_j}\right)\lambda_{cd}\,,\\&g_{cd}^B=0\,,\;\boldsymbol{g}_{cr_i}:={}^0\tilde{\boldsymbol{r}}_{S_i}-{}^0\boldsymbol{r}_{S_i}=\boldsymbol{0}\,,\;\boldsymbol{g}_{c\gamma_i}:=\tilde{\boldsymbol{\gamma}}_i-\boldsymbol{\gamma}_i=\boldsymbol{0}\,,\;\boldsymbol{g}_{c\gamma_j}:=\tilde{\boldsymbol{\gamma}}_j-\boldsymbol{\gamma}_j=\boldsymbol{0}\,.\end{aligned}\tag{42}$$

The equations of motion for the coupling bodies $i$ and $j$ are defined by Eqs. (26) and (27) together with Eq. (42). Applying a co-simulation approach (weak coupling approach), the subsystems are integrated independently from $T_N$ to $T_{N+1}$. As a consequence, the state variables $\boldsymbol{z}_j$ are not available in subsystem 1 and the state variables $\boldsymbol{z}_i$ are not accessible in subsystem 2. For that reason, the state variables $\boldsymbol{\gamma}_j$ are replaced by the additional coupling variables $\tilde{\boldsymbol{\gamma}}_j$ in subsystem 1. In subsystem 2, the state variables ${}^0\boldsymbol{r}_{S_i}$ and $\boldsymbol{\gamma}_i$ are replaced by the additional coupling variables ${}^0\tilde{\boldsymbol{r}}_{S_i}$ and $\tilde{\boldsymbol{\gamma}}_i$. Due to the additional coupling variables, the additional coupling conditions $\boldsymbol{g}_{cr_i}$, $\boldsymbol{g}_{c\gamma_i}$ and $\boldsymbol{g}_{c\gamma_j}$ – representing 9 scalar coupling conditions – have to be added to the decomposed system.

According to Sect. 3.3.1, the input vectors for the coupling bodies $i$ and $j$ are given by $\tilde{\boldsymbol{u}}_j=\left(\lambda_{cd}\;\;\tilde{\boldsymbol{\gamma}}_j\right)^T\in\mathbb{R}^4$ and $\tilde{\boldsymbol{u}}_i=\left(\lambda_{cd}\;\;{}^0\tilde{\boldsymbol{r}}_{S_i}\;\;\tilde{\boldsymbol{\gamma}}_i\right)^T\in\mathbb{R}^7$. The vector collecting the coupling equations is given by $\boldsymbol{g}_c^B=\left(g_{cd}^B\;\;\boldsymbol{g}_{cr_i}\;\;\boldsymbol{g}_{c\gamma_i}\;\;\boldsymbol{g}_{c\gamma_j}\right)^T\in\mathbb{R}^{10}$.

**Semi-implicit co-simulation approach based on weighted multipliers:**
For the weighted multiplier co-simulation method, the constraint equation (37) is complemented by the coupling conditions on velocity and on acceleration level

$$\begin{aligned}&\left[(\boldsymbol{r}_{S_i}+\boldsymbol{r}_{C_i})-\left(\boldsymbol{r}_{S_j}+\boldsymbol{r}_{C_j}\right)\right]\cdot\boldsymbol{e}_j=0\,,\\&\frac{d}{dt}\left\{\left[(\boldsymbol{r}_{S_i}+\boldsymbol{r}_{C_i})-\left(\boldsymbol{r}_{S_j}+\boldsymbol{r}_{C_j}\right)\right]\cdot\boldsymbol{e}_j\right\}=0\,,\\&\frac{d^2}{dt^2}\left\{\left[(\boldsymbol{r}_{S_i}+\boldsymbol{r}_{C_i})-\left(\boldsymbol{r}_{S_j}+\boldsymbol{r}_{C_j}\right)\right]\cdot\boldsymbol{e}_j\right\}=0\,.\end{aligned}\tag{43}$$

Representing the vectors in Eq. (43) with respect to the system $K_0$ yields

$$\begin{aligned}g_{cd}:=&\left[\left({}^0\boldsymbol{r}_{S_i}+{}^{0i}\boldsymbol{T}(\boldsymbol{\gamma}_i)^i\boldsymbol{r}_{C_i}\right)-\left({}^0\boldsymbol{r}_{S_j}+{}^{0j}\boldsymbol{T}(\boldsymbol{\gamma}_j)^j\boldsymbol{r}_{C_j}\right)\right]\cdot{}^{0j}\boldsymbol{T}(\boldsymbol{\gamma}_j)^j\boldsymbol{e}_j=0\,,\\\dot{g}_{cd}:=&\frac{d}{dt}\left\{\left[\left({}^0\boldsymbol{r}_{S_i}+{}^{0i}\boldsymbol{T}(\boldsymbol{\gamma}_i)^i\boldsymbol{r}_{C_i}\right)-\left({}^0\boldsymbol{r}_{S_j}+{}^{0j}\boldsymbol{T}(\boldsymbol{\gamma}_j)^j\boldsymbol{r}_{C_j}\right)\right]\cdot{}^{0j}\boldsymbol{T}(\boldsymbol{\gamma}_j)^j\boldsymbol{e}_j\right\}=0\,,\\\ddot{g}_{cd}:=&\frac{d^2}{dt^2}\left\{\left[\left({}^0\boldsymbol{r}_{S_i}+{}^{0i}\boldsymbol{T}(\boldsymbol{\gamma}_i)^i\boldsymbol{r}_{C_i}\right)-\left({}^0\boldsymbol{r}_{S_j}+{}^{0j}\boldsymbol{T}(\boldsymbol{\gamma}_j)^j\boldsymbol{r}_{C_j}\right)\right]\cdot{}^{0j}\boldsymbol{T}(\boldsymbol{\gamma}_j)^j\boldsymbol{e}_j\right\}=0\,.\end{aligned}\tag{44}$$

 

Connecting $C_i$ and $C_j$ by an inplane joint and applying the weighted multiplier co-simulation approach, the coupling forces/torques and the 12 scalar coupling conditions are defined by

$$
\begin{aligned}
&{}^0\boldsymbol{F}_{c_i} = {}^{0j}\boldsymbol{T}(\tilde{\boldsymbol{\gamma}}_j)\,{}^j\boldsymbol{e}_j\,\lambda_{cd}\,, \qquad {}^i\boldsymbol{M}_{c_i} = {}^i\boldsymbol{r}_{C_i} \times {}^{ij}\boldsymbol{T}(\boldsymbol{\gamma}_i,\tilde{\boldsymbol{\gamma}}_j)\,{}^j\boldsymbol{e}_j\,\lambda_{cd}\,,\\
&{}^0\boldsymbol{F}_{c_j} = -{}^{0j}\boldsymbol{T}(\boldsymbol{\gamma}_j)^j\boldsymbol{e}_j\,\lambda_{cd}\,, \qquad {}^j\boldsymbol{M}_{c_j} = {}^j\boldsymbol{e}_j \times {}^{j0}\boldsymbol{T}(\boldsymbol{\gamma}_j)\left({}^0\tilde{\boldsymbol{r}}_{S_i} + {}^{0i}\boldsymbol{T}(\tilde{\boldsymbol{\gamma}}_i)\,{}^i\boldsymbol{r}_{C_i} - {}^0\boldsymbol{r}_{S_j}\right)\lambda_{cd}\,,\\
&g_{cd} = 0\,,\ \dot{g}_{cd} = 0\,,\ \ddot{g}_{cd} = 0\,,\ \boldsymbol{g}_{cr_i} := {}^0\tilde{\boldsymbol{r}}_{S_i} - {}^0\boldsymbol{r}_{S_i} = \boldsymbol{0}\,,\ \boldsymbol{g}_{c\gamma_i} := \tilde{\boldsymbol{\gamma}}_i - \boldsymbol{\gamma}_i = \boldsymbol{0}\,,\ \boldsymbol{g}_{c\gamma_j} := \tilde{\boldsymbol{\gamma}}_j - \boldsymbol{\gamma}_j = \boldsymbol{0}\,. \qquad (45)
\end{aligned}
$$

According to Sect. 3.3.2, the input vectors for the coupling bodies $i$ and $j$ are given by $\tilde{\boldsymbol{u}}_j = (\lambda_{cd}\ \ \tilde{\boldsymbol{\gamma}}_j)^T \in \mathbb{R}^4$ and $\tilde{\boldsymbol{u}}_i = (\lambda_{cd}\ \ {}^0\tilde{\boldsymbol{r}}_{S_i}\ \ \tilde{\boldsymbol{\gamma}}_i)^T \in \mathbb{R}^7$. The 3 vectors collecting the coupling equations are given by $\boldsymbol{g}_c^{pos} = \begin{pmatrix} g_{cd} & \boldsymbol{g}_{cr_i} & \boldsymbol{g}_{c\gamma_i} & \boldsymbol{g}_{c\gamma_j}\end{pmatrix}^T$, $\boldsymbol{g}_c^{vel} = \begin{pmatrix}\dot{g}_{cd} & \boldsymbol{g}_{cr_i} & \boldsymbol{g}_{c\gamma_i} & \boldsymbol{g}_{c\gamma_j}\end{pmatrix}^T$, $\boldsymbol{g}_c^{acc} = \begin{pmatrix}\ddot{g}_{cd} & \boldsymbol{g}_{cr_i} & \boldsymbol{g}_{c\gamma_i} & \boldsymbol{g}_{c\gamma_j}\end{pmatrix}^T \in \mathbb{R}^{10}$.

### 3.2.3 Perpendicular joint

The third fundamental joint is the *perpendicular joint*, defined by the coupling condition

$$\boldsymbol{e}_i \cdot \boldsymbol{e}_j = 0\,, \qquad (46)$$

where $\boldsymbol{e}_i$ and $\boldsymbol{e}_j$ denote arbitrary unit vectors fixed at body $i$ and body $j$, respectively. Evaluating the vectors in Eq. (46) with respect to the system $K_0$ yields

$$g_{cp} := {}^{0i}\boldsymbol{T}(\boldsymbol{\gamma}_i)^i\boldsymbol{e}_i \cdot {}^{0j}\boldsymbol{T}(\boldsymbol{\gamma}_j)^j\boldsymbol{e}_j = 0\,. \qquad (47)$$

The constraint forces and constraint torques resulting from the constraint equation (47) read as

$$
\begin{aligned}
&{}^0\boldsymbol{F}_{c_i} = \boldsymbol{0}\,, \qquad {}^i\boldsymbol{M}_{c_i} = {}^i\boldsymbol{e}_i \times {}^{ij}\boldsymbol{T}(\boldsymbol{\gamma}_i,\boldsymbol{\gamma}_j)\,{}^j\boldsymbol{e}_j\,\lambda_{cp}\,,\\
&{}^0\boldsymbol{F}_{c_j} = \boldsymbol{0}\,, \qquad {}^j\boldsymbol{M}_{c_j} = {}^j\boldsymbol{e}_j \times {}^{ji}\boldsymbol{T}(\boldsymbol{\gamma}_i,\boldsymbol{\gamma}_j)\,{}^i\boldsymbol{e}_i\,\lambda_{cp}\,, \qquad (48)
\end{aligned}
$$

where $\lambda_{cp}$ represents the Lagrange multiplier.

**Semi-implicit co-simulation approach based on Baumgarte-stabilization:**
Using the Baumgarte-stabilization approach, the constraint equation (46) is replaced by the coupling condition

$$\boldsymbol{e}_i \cdot \boldsymbol{e}_j + \beta \cdot \frac{d}{dt}\left\{\boldsymbol{e}_i \cdot \boldsymbol{e}_j\right\} + \gamma \cdot \frac{d^2}{dt^2}\left\{\boldsymbol{e}_i \cdot \boldsymbol{e}_j\right\} = \boldsymbol{0}\,. \qquad (49)$$

Decomposing the vectors with respect to $K_0$ yields

$$
\begin{aligned}
g_{cp}^B :=\ & {}^{0i}\boldsymbol{T}(\boldsymbol{\gamma}_i)^i\boldsymbol{e}_i \cdot {}^{0j}\boldsymbol{T}(\boldsymbol{\gamma}_j)^j\boldsymbol{e}_j\\
&+ \beta \cdot \frac{d}{dt}\left\{{}^{0i}\boldsymbol{T}(\boldsymbol{\gamma}_i)^i\boldsymbol{e}_i \cdot {}^{0j}\boldsymbol{T}(\boldsymbol{\gamma}_j)^j\boldsymbol{e}_j\right\} + \gamma \cdot \frac{d^2}{dt^2}\left\{{}^{0i}\boldsymbol{T}(\boldsymbol{\gamma}_i)^i\boldsymbol{e}_i \cdot {}^{0j}\boldsymbol{T}(\boldsymbol{\gamma}_j)^j\boldsymbol{e}_j\right\} = 0\,. \qquad (50)
\end{aligned}
$$

Connecting subsystem 1 and subsystem 2 by a perpendicular joint and applying the Baumgarte-stabilization approach, the coupling forces/torques and the 7 scalar coupling conditions are given by

$$
\begin{aligned}
&{}^0\boldsymbol{F}_{c_i} = \boldsymbol{0}\,, \qquad {}^i\boldsymbol{M}_{c_i} = {}^i\boldsymbol{e}_i \times {}^{ij}\boldsymbol{T}(\boldsymbol{\gamma}_i,\tilde{\boldsymbol{\gamma}}_j)\,{}^j\boldsymbol{e}_j\,\lambda_{cp}\,,\\
&{}^0\boldsymbol{F}_{c_j} = \boldsymbol{0}\,, \qquad {}^j\boldsymbol{M}_{c_j} = {}^j\boldsymbol{e}_j \times {}^{ji}\boldsymbol{T}(\tilde{\boldsymbol{\gamma}}_i,\boldsymbol{\gamma}_j)\,{}^i\boldsymbol{e}_i\,\lambda_{cp}\,,\\
&g_{cp}^B = 0\,,\ \boldsymbol{g}_{c\gamma_i} := \tilde{\boldsymbol{\gamma}}_i - \boldsymbol{\gamma}_i = \boldsymbol{0}\,,\ \boldsymbol{g}_{c\gamma_j} := \tilde{\boldsymbol{\gamma}}_j - \boldsymbol{\gamma}_j = \boldsymbol{0}\,. \qquad (51)
\end{aligned}
$$

Equations (26), (27), and (51) represent the equations of motion for the coupling bodies $i$ and $j$. For the perpendicular joint, 6 additional coupling variables ($\tilde{\boldsymbol{\gamma}}_i$ and $\tilde{\boldsymbol{\gamma}}_j$) and 6 additional scalar coupling conditions ($\boldsymbol{g}_{c\gamma_i}$ and $\boldsymbol{g}_{c\gamma_j}$) have to be defined.

According to Sect. 3.3.1, the input vectors for the coupling bodies $i$ and $j$ are given by $\tilde{\boldsymbol{u}}_j = (\lambda_{cp}\ \ \tilde{\boldsymbol{\gamma}}_j)^T \in \mathbb{R}^4$ and $\tilde{\boldsymbol{u}}_i = (\lambda_{cp}\ \ \tilde{\boldsymbol{\gamma}}_i)^T \in \mathbb{R}^4$. The vector collecting the coupling equations is given by $\boldsymbol{g}_c^B = \begin{pmatrix} g_{cp}^B & \boldsymbol{g}_{c\gamma_i} & \boldsymbol{g}_{c\gamma_j}\end{pmatrix}^T \in \mathbb{R}^7$.

**Semi-implicit co-simulation approach based on weighted multipliers:**
For the weighted multiplier co-simulation method, the constraint equation (46) is complemented by the coupling conditions on velocity and on acceleration level

$$\boldsymbol{e}_i \cdot \boldsymbol{e}_j = 0\,, \quad \frac{d}{dt}\left\{\boldsymbol{e}_i \cdot \boldsymbol{e}_j\right\} = 0\,, \quad \frac{d^2}{dt^2}\left\{\boldsymbol{e}_i \cdot \boldsymbol{e}_j\right\} = 0\,. \tag{52}$$

Representing the vectors in Eq. (52) with respect to the system $K_0$ yields

$$\begin{aligned} g_{cp} &:= {}^{0i}\boldsymbol{T}(\boldsymbol{\gamma}_i)^i\boldsymbol{e}_i \cdot {}^{0j}\boldsymbol{T}(\boldsymbol{\gamma}_j)^j\boldsymbol{e}_j = 0\,, \\ \dot{g}_{cp} &:= \frac{d}{dt}\left\{{}^{0i}\boldsymbol{T}(\boldsymbol{\gamma}_i)^i\boldsymbol{e}_i \cdot {}^{0j}\boldsymbol{T}(\boldsymbol{\gamma}_j)^j\boldsymbol{e}_j\right\} = 0\,, \\ \ddot{g}_{cp} &:= \frac{d^2}{dt^2}\left\{{}^{0i}\boldsymbol{T}(\boldsymbol{\gamma}_i)^i\boldsymbol{e}_i \cdot {}^{0j}\boldsymbol{T}(\boldsymbol{\gamma}_j)^j\boldsymbol{e}_j\right\} = 0\,. \end{aligned} \tag{53}$$

Connecting $C_i$ and $C_j$ by a perpendicular joint and applying the weighted multiplier co-simulation approach, the coupling forces/torques and the 9 scalar coupling conditions are defined by

$$\begin{aligned} &{}^0\boldsymbol{F}_{c_i} = \boldsymbol{0}\,, \qquad {}^i\boldsymbol{M}_{c_i} = {}^i\boldsymbol{e}_i \times {}^{ij}\boldsymbol{T}(\boldsymbol{\gamma}_i, \tilde{\boldsymbol{\gamma}}_j)\,{}^j\boldsymbol{e}_j\,\lambda_{cp}\,, \\ &{}^0\boldsymbol{F}_{c_j} = \boldsymbol{0}\,, \qquad {}^j\boldsymbol{M}_{c_j} = {}^j\boldsymbol{e}_j \times {}^{ji}\boldsymbol{T}(\tilde{\boldsymbol{\gamma}}_i, \boldsymbol{\gamma}_j)\,{}^i\boldsymbol{e}_i\,\lambda_{cp}\,, \\ &g_{cp} = 0\,,\ \dot{g}_{cp} = 0\,,\ \ddot{g}_{cp} = 0\,,\ \boldsymbol{g}_{c\gamma_i} := \tilde{\boldsymbol{\gamma}}_i - \boldsymbol{\gamma}_i = \boldsymbol{0}\,,\ \boldsymbol{g}_{c\gamma_j} := \tilde{\boldsymbol{\gamma}}_j - \boldsymbol{\gamma}_j = \boldsymbol{0}\,. \end{aligned} \tag{54}$$

According to Sect. 3.3.2, the input vectors for the coupling bodies $i$ and $j$ are given by $\tilde{\boldsymbol{u}}_j = (\lambda_{cp}\ \ \tilde{\boldsymbol{\gamma}}_j)^T \in \mathbb{R}^4$ and $\tilde{\boldsymbol{u}}_i = (\lambda_{cp}\ \ \tilde{\boldsymbol{\gamma}}_i)^T \in \mathbb{R}^4$. The 3 vectors collecting the coupling equations are given by $\boldsymbol{g}_c^{pos} = \begin{pmatrix} g_{cp} & \boldsymbol{g}_{c\gamma_i} & \boldsymbol{g}_{c\gamma_j} \end{pmatrix}^T$, $\boldsymbol{g}_c^{vel} = \begin{pmatrix} \dot{g}_{cp} & \boldsymbol{g}_{c\gamma_i} & \boldsymbol{g}_{c\gamma_j} \end{pmatrix}^T$, $\boldsymbol{g}_c^{acc} = \begin{pmatrix} \ddot{g}_{cp} & \boldsymbol{g}_{c\gamma_i} & \boldsymbol{g}_{c\gamma_j} \end{pmatrix}^T \in \mathbb{R}^7$.

### 3.3 General integration scheme for predictor/corrector co-simulation approaches

#### 3.3.1 Method 1: Semi-implicit co-simulation approach based on Baumgarte-stabilization

As already outlined in Sect. 2 in connection with the 1-DOF test model, the semi-implicit co-simulation approach is accomplished in 3 steps, which are in the following described for the general case that 2 arbitrary mechanical subsystems are coupled. Firstly, we define some auxiliary vectors. The coupling (input) vector $\tilde{\boldsymbol{u}}_j = (\tilde{u}_{j1}\,\tilde{u}_{j2}\,\ldots\,\tilde{u}_{jn_{\tilde{u}j}})^T \in \mathbb{R}^{n_{\tilde{u}j}}$ contains the $n_{\tilde{u}j}$ coupling variables for the coupling body $i$. The coupling (input) vector $\tilde{\boldsymbol{u}}_i = (\tilde{u}_{i1}\,\tilde{u}_{i2}\,\ldots\,\tilde{u}_{in_{\tilde{u}i}})^T \in \mathbb{R}^{n_{\tilde{u}i}}$ collects the $n_{\tilde{u}i}$ coupling variables for the coupling body $j$. Both vectors are combined in the resultant coupling vector $\tilde{\boldsymbol{u}}_c = \begin{pmatrix} \tilde{\boldsymbol{u}}_j & \tilde{\boldsymbol{u}}_i \end{pmatrix}^T \in \mathbb{R}^{n_{\tilde{u}j}+n_{\tilde{u}i}}$. The coupling conditions are formally arranged in the vector $\boldsymbol{g}_c^B = \begin{pmatrix} g_{c1} & g_{c2} & \ldots & g_{cn_g} \end{pmatrix}^T \in \mathbb{R}^{n_g}$. For example, coupling the bodies $i$ and $j$ by an atpoint joint and by a perpendicular joint, the coupling variables and coupling conditions are given by: $\tilde{\boldsymbol{u}}_j = ({}^0\boldsymbol{\lambda}_{ca}\ \ \lambda_{cp}\ \ \tilde{\boldsymbol{\gamma}}_j)^T \in \mathbb{R}^7$, $\tilde{\boldsymbol{u}}_i = ({}^0\boldsymbol{\lambda}_{ca}\ \ \lambda_{cp}\ \ \tilde{\boldsymbol{\gamma}}_i)^T \in \mathbb{R}^7$, and $\boldsymbol{g}_c^B = \begin{pmatrix} \boldsymbol{g}_{ca}^B & g_{cp}^B & \boldsymbol{g}_{c\gamma_i} & \boldsymbol{g}_{c\gamma_j} \end{pmatrix}^T \in \mathbb{R}^{10}$.

In order to explain the semi-implicit coupling approach, we consider the general macro-time step from $T_N$ to $T_{N+1}$. In Sect. 2, the coupling variable has been approximated by a constant polynomial. Now, we discuss the general case that the coupling variables $\tilde{\boldsymbol{u}}_j$ and $\tilde{\boldsymbol{u}}_i$ are approximated by polynomials of degree $k$. At the beginning of the macro-time step, the state variables of the subsystems and the coupling variables are assumed to be known

$$\hat{\boldsymbol{z}}_1\,(t = T_N) = \hat{\boldsymbol{z}}_{1,N}\,,\ \ \hat{\boldsymbol{z}}_2\,(t = T_N) = \hat{\boldsymbol{z}}_{2,N}\,, \tag{55a}$$

$$\tilde{\boldsymbol{u}}_j\,(t = T_N) = \tilde{\boldsymbol{u}}_{j,N}\,,\ \ \tilde{\boldsymbol{u}}_i\,(t = T_N) = \tilde{\boldsymbol{u}}_{i,N}\,. \tag{55b}$$

**Step 1: Predictor step**

- In the predictor step, both subsystems integrate from $T_N$ to $T_{N+1}$ using extrapolated coupling variables. In order to extrapolate the coupling variables, each component of the coupling vectors $\tilde{\boldsymbol{u}}_j$ and $\tilde{\boldsymbol{u}}_i$ has to be approximated. Here, Lagrange polynomials are used for extrapolating the coupling variables. The Lagrange polynomial of degree $k$ is defined by $k+1$ sampling points. In the predictor step, these sampling points are defined by the macro-time points $T_N, T_{N-1}, \ldots, T_{N-k}$. Regarding, for example, the $m^{th}$ $(1 \le m \le n_{\tilde{u}j})$ coupling variable

 

$\tilde{u}_{jm}$, the corresponding predictor polynomial $P^p_{\tilde{u}_{jm}}(t)$ for the macro-time interval $[T_N, T_{N+1}]$ is defined by the $k+1$ sampling points $(T_N, \tilde{u}_{jm,N})$, $(T_{N-1}, \tilde{u}_{jm,N-1})$, …, $(T_{N-k}, \tilde{u}_{jm,N-k})$ and may simply be abbreviated by $P^p_{\tilde{u}_{jm}}[(T_N, \tilde{u}_{jm,N}), (T_{N-1}, \tilde{u}_{jm,N-1}), \ldots, (T_{N-k}, \tilde{u}_{jm,N-k}); t]$. The extrapolation polynomials of the coupling variables $\tilde{\boldsymbol{u}}_j$ for subsystem 1 are formally collected into the vector $\boldsymbol{P}^p_j \in \mathbb{R}^{n_{\tilde{u}j}}$. The corresponding extrapolation polynomials for $\tilde{\boldsymbol{u}}_i$ in subsystem 2 are arranged into the vector $\boldsymbol{P}^p_i \in \mathbb{R}^{n_{\tilde{u}i}}$.

- Using the predicted (extrapolated) coupling variables

$$\tilde{\boldsymbol{u}}^p_j(t) = \boldsymbol{P}^p_j\left[\left(T_N, \tilde{\boldsymbol{u}}_{j,N}\right), \left(T_{N-1}, \tilde{\boldsymbol{u}}_{j,N-1}\right), \ldots, \left(T_{N-k}, \tilde{\boldsymbol{u}}_{j,N-k}\right); t\right] \text{ and}$$
$$\tilde{\boldsymbol{u}}^p_i(t) = \boldsymbol{P}^p_i\left[\left(T_N, \tilde{\boldsymbol{u}}_{i,N}\right), \left(T_{N-1}, \tilde{\boldsymbol{u}}_{i,N-1}\right), \ldots, \left(T_{N-k}, \tilde{\boldsymbol{u}}_{i,N-k}\right); t\right], \tag{56}$$

the integration of subsystem 1 and subsystem 2 from $T_N$ to $T_{N+1}$ with initial conditions (55a) yields the predicted state variables at the macro-time point $T_{N+1}$

$$\hat{\boldsymbol{z}}^p_{1,N+1} = \hat{\boldsymbol{z}}_{1,N+1}(\tilde{\boldsymbol{u}}^p_j), \qquad \hat{\boldsymbol{z}}^p_{2,N+1} = \hat{\boldsymbol{z}}_{2,N+1}(\tilde{\boldsymbol{u}}^p_i). \tag{57}$$

- Inserting the predicted state variables from Eq. (57) into the equations of motion (26) and (27) yields the predicted accelerations at the macro-time point $T_{N+1}$

$$\boldsymbol{a}^p_{i,N+1} = \boldsymbol{a}_{i,N+1}(\hat{\boldsymbol{z}}^p_{1,N+1}), \qquad \boldsymbol{a}^p_{j,N+1} = \boldsymbol{a}_{j,N+1}(\hat{\boldsymbol{z}}^p_{2,N+1}). \tag{58}$$

**Step 2: Calculation of corrected coupling variables**

- The integration of subsystem 1 and subsystem 2 from $T_N$ to $T_{N+1}$ is repeated. Therefore, the same predictor polynomials are used as in step 1, however with two exceptions. Firstly, the $m^{th}$ $(1 \le m \le n_{\tilde{u}j})$ component of $\boldsymbol{P}^p_j$ is replaced by the perturbed predicted (interpolation) polynomial $P^{pp_m}_{\tilde{u}_{jm}}[(T_{N+1}, \tilde{u}^p_{jm,N+1} + \Delta u_m), (T_N, \tilde{u}_{jm,N}), \ldots, (T_{N-k+1}, \tilde{u}_{jm,N-k+1}); t]$, see Fig. 4. Secondly, the $n^{th}$ $(1 \le n \le n_{\tilde{u}i})$ component of $\boldsymbol{P}^p_i$ is replaced by the perturbed predicted (interpolation) polynomial $P^{pp_n}_{\tilde{u}_{in}}[(T_{N+1}, \tilde{u}^p_{in,N+1} + \Delta u_n), (T_N, \tilde{u}_{in,N}), \ldots, (T_{N-k+1}, \tilde{u}_{in,N-k+1}); t]$. The vectors collecting the approximation polynomials with the perturbed components $m$ and $n$ are denoted by $\boldsymbol{P}^{pp_m}_j$ and $\boldsymbol{P}^{pp_n}_i$. It should be mentioned that $\Delta u_m$ and $\Delta u_n$ are user-defined increments.
- Using the perturbed predicted coupling variables

$$\tilde{\boldsymbol{u}}^{pp_m}_j(t) = \boldsymbol{P}^{pp_m}_j\left[\left(T_{N+1}, \tilde{u}^p_{jm,N+1} + \Delta u_m\right), \left(T_N, \tilde{\boldsymbol{u}}_{j,N}\right), \left(T_{N-1}, \tilde{\boldsymbol{u}}_{j,N-1}\right), \ldots; t\right] \text{ and}$$
$$\tilde{\boldsymbol{u}}^{pp_n}_i(t) = \boldsymbol{P}^{pp_n}_i\left[\left(T_{N+1}, \tilde{u}^p_{in,N+1} + \Delta u_n\right), \left(T_N, \tilde{\boldsymbol{u}}_{i,N}\right), \left(T_{N-1}, \tilde{\boldsymbol{u}}_{i,N-1}\right), \ldots; t\right], \tag{59}$$

the integration of subsystem 1 and subsystem 2 from $T_N$ to $T_{N+1}$ with initial conditions (55a) yields the perturbed predicted state variables at the macro-time point $T_{N+1}$

$$\hat{\boldsymbol{z}}^{pp_m}_{1,N+1} = \hat{\boldsymbol{z}}_{1,N+1}(\tilde{\boldsymbol{u}}^{pp_m}_j), \qquad \hat{\boldsymbol{z}}^{pp_n}_{2,N+1} = \hat{\boldsymbol{z}}_{2,N+1}(\tilde{\boldsymbol{u}}^{pp_n}_i). \tag{60}$$

- Inserting the perturbed predicted state variables from Eq. (60) into the equations of motion (26) and (27) yields the perturbed predicted accelerations at the macro-time point $T_{N+1}$

$$\boldsymbol{a}^{pp_m}_{i,N+1} = \boldsymbol{a}_{i,N+1}(\hat{\boldsymbol{z}}^{pp_m}_{1,N+1}), \qquad \boldsymbol{a}^{pp_n}_{j,N+1} = \boldsymbol{a}_{j,N+1}(\hat{\boldsymbol{z}}^{pp_n}_{2,N+1}). \tag{61}$$

- With the predicted and the perturbed predicted state variables, the partial derivatives of the states with respect to the coupling variables can approximately be calculated by finite differences. For the partial derivative of the $\mu^{th}$ $(1 \le \mu \le 12)$ component of $\boldsymbol{z}_i$ with respect to the $m^{th}$ component of $\tilde{\boldsymbol{u}}_j$ we get

$$\left.\frac{\partial z_{i\mu,N+1}}{\partial \tilde{u}_{jm,N+1}}\right|_{\tilde{\boldsymbol{u}}^p_{c,N+1}} \approx \frac{z_{i\mu,N+1}\left(\tilde{\boldsymbol{u}}^{pp_m}_j\right) - z_{i\mu,N+1}\left(\tilde{\boldsymbol{u}}^p_j\right)}{\Delta u_m}. \tag{62}$$

Analogously, the partial derivative of the $\nu^{th}$ $(1 \le \nu \le 12)$ component of $\boldsymbol{z}_j$ with respect to the $n^{th}$ component of $\tilde{\boldsymbol{u}}_i$ can be approximated by

$$\left.\frac{\partial z_{j\nu,N+1}}{\partial \tilde{u}_{in,N+1}}\right|_{\tilde{\boldsymbol{u}}^p_{c,N+1}} \approx \frac{z_{j\nu,N+1}\left(\tilde{\boldsymbol{u}}^{pp_n}_i\right) - z_{j\nu,N+1}\left(\tilde{\boldsymbol{u}}^p_i\right)}{\Delta u_n}. \tag{63}$$

- In a similar manner, the partial derivatives of the accelerations $\boldsymbol{a}_i$ and $\boldsymbol{a}_j$ with respect to the coupling variables $\tilde{\boldsymbol{u}}_j$ and $\tilde{\boldsymbol{u}}_i$ can be calculated using Eqs. (58) and (61).
- Making use of the partial derivatives, corrected (i.e. improved) values for the coupling variables at the time point $T_{N+1}$ can be obtained. Regarding the fixed macro-time point $T_{N+1}$, $\boldsymbol{g}^B_{c,N+1}$ can formally be considered as a function of the coupling variables $\tilde{\boldsymbol{u}}_{c,N+1}$, i.e.

$$\boldsymbol{g}^B_{c,N+1}\left(\tilde{\boldsymbol{u}}_{c,N+1}\right) . \tag{64}$$

Choosing $\tilde{\boldsymbol{u}}^p_{c,N+1}$ as expansion point and neglecting higher order terms $\mathcal{O}(\tilde{\boldsymbol{u}}^2_{c,N+1})$, a Taylor series expansion of $\boldsymbol{g}^B_{c,N+1}\left(\tilde{\boldsymbol{u}}_{c,N+1}\right)$ with respect to $\tilde{\boldsymbol{u}}_{c,N+1}$ yields the linearized coupling conditions

$$\boldsymbol{g}^{B,linear}_{c,N+1}\left(\tilde{\boldsymbol{u}}_{c,N+1}\right) := \boldsymbol{g}^B_{c,N+1}\left(\tilde{\boldsymbol{u}}^p_{c,N+1}\right) + \left.\frac{\partial \boldsymbol{g}^B_{c,N+1}}{\partial \tilde{\boldsymbol{u}}_{c,N+1}}\right|_{\tilde{\boldsymbol{u}}^p_{c,N+1}} \cdot \left(\tilde{\boldsymbol{u}}_{c,N+1} - \tilde{\boldsymbol{u}}^p_{c,N+1}\right) = \boldsymbol{0} . \tag{65}$$

In general, the coupling conditions are functions of the state variables $\boldsymbol{z}_c$ and (for $\gamma \neq 0$) of the accelerations $\boldsymbol{a}_c$, i.e.

$$\boldsymbol{g}^B_{c,N+1}\left(\tilde{\boldsymbol{u}}_{c,N+1}\right) = \boldsymbol{g}^B_{c,N+1}\left(\boldsymbol{z}_{c,N+1}(\tilde{\boldsymbol{u}}_{c,N+1}),\, \boldsymbol{a}_{c,N+1}(\tilde{\boldsymbol{u}}_{c,N+1})\right) . \tag{66}$$

Therefore, the Jacobian $\boldsymbol{G}^B$ can be written as

$$\boldsymbol{G}^B = \left.\frac{\partial \boldsymbol{g}^B_{c,N+1}}{\partial \tilde{\boldsymbol{u}}_{c,N+1}}\right|_{\tilde{\boldsymbol{u}}^p_{c,N+1}} = \left.\frac{\partial \boldsymbol{g}^B_{c,N+1}}{\partial \boldsymbol{z}_{c,N+1}} \frac{\partial \boldsymbol{z}_{c,N+1}}{\partial \tilde{\boldsymbol{u}}_{c,N+1}}\right|_{\tilde{\boldsymbol{u}}^p_{c,N+1}} + \left.\frac{\partial \boldsymbol{g}^B_{c,N+1}}{\partial \boldsymbol{a}_{c,N+1}} \frac{\partial \boldsymbol{a}_{c,N+1}}{\partial \tilde{\boldsymbol{u}}_{c,N+1}}\right|_{\tilde{\boldsymbol{u}}^p_{c,N+1}} , \tag{67}$$

where the partial derivatives $\left.\frac{\partial \boldsymbol{z}_{c,N+1}}{\partial \tilde{\boldsymbol{u}}_{c,N+1}}\right|_{\tilde{\boldsymbol{u}}^p_{c,N+1}}$ and $\left.\frac{\partial \boldsymbol{a}_{c,N+1}}{\partial \tilde{\boldsymbol{u}}_{c,N+1}}\right|_{\tilde{\boldsymbol{u}}^p_{c,N+1}}$ can approximately be calculated by finite differences, see above.

- Generally, the predicted states and accelerations do not fulfill the coupling conditions, i.e. $\boldsymbol{g}^B_{c,N+1}(\boldsymbol{z}_{c,N+1}(\tilde{\boldsymbol{u}}^p_{c,N+1}),\, \boldsymbol{a}_{c,N+1}(\tilde{\boldsymbol{u}}^p_{c,N+1})) \neq \boldsymbol{0}$. Improved coupling variables, which fulfill the linearized coupling conditions, can be derived by solving Eq. (65) for $\tilde{\boldsymbol{u}}_{c,N+1}$, which yields

$$\tilde{\boldsymbol{u}}_{c,N+1} = \tilde{\boldsymbol{u}}^p_{c,N+1} - \boldsymbol{G}^{B^{-1}} \cdot \boldsymbol{g}_{c,N+1}\left(\tilde{\boldsymbol{u}}^p_{c,N+1}\right) . \tag{68}$$

- Remark: For the approximation of the partial derivatives with finite differences, the increment $\Delta u_m$ has to be specified, see Eq. 62. Instead of using the same increment for all coupling variables and instead of using constant increments, it might be more suitable to use different and variable increments. For instance, $\Delta u_m = \varepsilon_m \cdot \max\left(1, |\tilde{u}_{jm,N}|\right)$ could be used, where $\varepsilon_m$ denotes a small user-defined parameter (e.g. $\varepsilon_m = 10^{-5}$; maybe a function of the macro-step size) to be specified individually for each component $\tilde{u}_{jm}$ of the coupling vector.

**Step 3: Corrector step**

- Using the corrected (interpolated) coupling variables (see also Fig. 4)

$$\begin{aligned}
&\tilde{\boldsymbol{u}}_j(t) = \boldsymbol{P}_j\left[\left(T_{N+1}, \tilde{\boldsymbol{u}}_{j,N+1}\right), \left(T_N, \tilde{\boldsymbol{u}}_{j,N}\right), \ldots, \left(T_{N-k+1}, \tilde{\boldsymbol{u}}_{j,N-k+1}\right); t\right] \text{ and} \\
&\tilde{\boldsymbol{u}}_i(t) = \boldsymbol{P}_i\left[\left(T_{N+1}, \tilde{\boldsymbol{u}}_{i,N+1}\right), \left(T_N, \tilde{\boldsymbol{u}}_{i,N}\right), \ldots, \left(T_{N-k+1}, \tilde{\boldsymbol{u}}_{i,N-k+1}\right); t\right] ,
\end{aligned} \tag{69}$$

the integration of subsystem 1 and subsystem 2 from $T_N$ to $T_{N+1}$ yields the corrected state variables at the macro-time point $T_{N+1}$

$$\hat{\boldsymbol{z}}_{1,N+1} = \hat{\boldsymbol{z}}_{1,N+1}(\tilde{\boldsymbol{u}}_j) , \qquad \hat{\boldsymbol{z}}_{2,N+1} = \hat{\boldsymbol{z}}_{2,N+1}(\tilde{\boldsymbol{u}}_i) . \tag{70}$$

#### 3.3.1.1 Semi-implicit index-3 co-simulation approach

For $\beta = \gamma = 0$, the semi-implicit co-simulation technique described above is a coupling approach on index-3 level. In this case, evaluation of Eqs. (58) and (61) can be omitted and only partial derivatives of the position variables with respect to the coupling variables have to be calculated (partial derivatives of the velocities and accelerations are not required).

#### 3.3.1.2 Semi-implicit index-2 co-simulation approach

Choosing $\beta > 0$ and $\gamma = 0$ yields a co-simulation approach on index-2 level. Applying the index-2 approach, evaluation of Eqs. (58) and (61) is not required. Furthermore, only partial derivatives of the state variables with respect to the coupling variables have to be calculated (partial derivatives of the accelerations are not required).

 

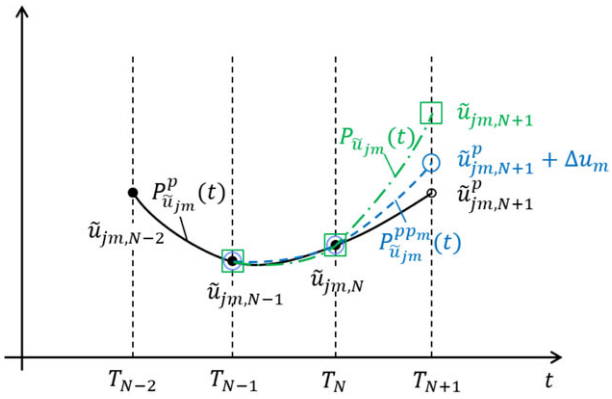


**Fig. 4** Illustration of the three different approximation polynomials (polynomial degree $k = 2$) for the coupling variable $\tilde{u}_{jm}(t)$: predictor (extrapolation) polynomial $P^p_{\tilde{u}_{jm}}(t)$, perturbed predicted (interpolation) polynomial $P^{pp_m}_{\tilde{u}_{jm}}(t)$, and corrector (interpolation) polynomial $P_{\tilde{u}_{jm}}(t)$.

#### 3.3.1.3 Semi-implicit index-1 co-simulation approach

Choosing $\beta > 0$ and $\gamma > 0$ yields an index-1 co-simulation approach.

### 3.3.2 Method 2: Semi-implicit co-simulation approach based on weighted multipliers

As already mentioned in Sect. 2, the weighted multiplier method is very similar to method 1. The two methods only differ in the calculation of the corrected coupling variables. The definition of the coupling (input) vectors $\tilde{\boldsymbol{u}}_j$ and $\tilde{\boldsymbol{u}}_i$ is equivalent to Sect. 3.3.1. According to Sect. 3.2, the coupling conditions can be subdivided into the primary coupling conditions $\boldsymbol{g}_{cprim} \in \{\boldsymbol{g}_{ca}, g_{cd}, g_{cp}\}$ and the additional coupling conditions $\boldsymbol{g}_{cadd} \in \left\{\boldsymbol{g}_{cr_i}, \boldsymbol{g}_{c\gamma_i}, \boldsymbol{g}_{c\gamma_j}\right\}$. For the weighted multiplier method, we define 3 different constraint vectors. The vector containing the primary coupling conditions on position level and the additional coupling conditions is denoted by $\boldsymbol{g}_c^{pos} = \left(\boldsymbol{g}_{cprim} \;\; \boldsymbol{g}_{cadd}\right)^T \in \mathbb{R}^{n_g}$. The vector collecting the primary coupling conditions on velocity level and the additional coupling conditions is termed by $\boldsymbol{g}_c^{vel} = \left(\dot{\boldsymbol{g}}_{cprim} \;\; \boldsymbol{g}_{cadd}\right)^T \in \mathbb{R}^{n_g}$. Finally, the vector containing the primary coupling conditions on acceleration level and the additional coupling conditions is represented by $\boldsymbol{g}_c^{acc} = \left(\ddot{\boldsymbol{g}}_{cprim} \;\; \boldsymbol{g}_{cadd}\right)^T \in \mathbb{R}^{n_g}$. For instance, connecting the bodies $i$ and $j$ by an atpoint joint and by a perpendicular joint, the coupling variables and coupling conditions are given by: $\tilde{\boldsymbol{u}}_j = \left({}^0\boldsymbol{\lambda}_{ca} \;\; \lambda_{cp} \;\; \tilde{\boldsymbol{\gamma}}_j\right)^T \in \mathbb{R}^7$, $\tilde{\boldsymbol{u}}_i = \left({}^0\boldsymbol{\lambda}_{ca} \;\; \lambda_{cp} \;\; \tilde{\boldsymbol{\gamma}}_i\right)^T \in \mathbb{R}^7$, and $\boldsymbol{g}_c^{pos} = \left(\boldsymbol{g}_{ca} \;\; g_{cp} \;\; \boldsymbol{g}_{c\gamma_i} \;\; \boldsymbol{g}_{c\gamma_j}\right)^T$, $\boldsymbol{g}_c^{vel} = \left(\dot{\boldsymbol{g}}_{ca} \;\; \dot{g}_{cp} \;\; \boldsymbol{g}_{c\gamma_i} \;\; \boldsymbol{g}_{c\gamma_j}\right)^T$, $\boldsymbol{g}_c^{acc} = \left(\ddot{\boldsymbol{g}}_{ca} \;\; \ddot{g}_{cp} \;\; \boldsymbol{g}_{c\gamma_i} \;\; \boldsymbol{g}_{c\gamma_j}\right)^T \in \mathbb{R}^{10}$.

**Step 1: Predictor step**

- The predictor step is equivalent to method 1 in Sect. 3.3.1.

**Step 2: Calculation of corrected coupling variables**

- Calculation of the partial derivatives according to Eqs. (62) and (63) is also equivalent to method 1 in Sect. 3.3.1.
- For calculating the corrected (improved) coupling variables $\tilde{\boldsymbol{u}}_{c,N+1}$, we consider the coupling conditions at the fixed macro-time point $T_{N+1}$ and interpret $\boldsymbol{g}^{pos}_{c,N+1}$, $\boldsymbol{g}^{vel}_{c,N+1}$ and $\boldsymbol{g}^{acc}_{c,N+1}$ as functions of the coupling variables $\tilde{\boldsymbol{u}}_{c,N+1}$

$$\boldsymbol{g}^{pos}_{c,N+1}\left(\tilde{\boldsymbol{u}}_{c,N+1}\right), \quad \boldsymbol{g}^{vel}_{c,N+1}\left(\tilde{\boldsymbol{u}}_{c,N+1}\right), \quad \boldsymbol{g}^{acc}_{c,N+1}\left(\tilde{\boldsymbol{u}}_{c,N+1}\right). \tag{71}$$

Next, the functions $\boldsymbol{g}^{pos}_{c,N+1}\left(\tilde{\boldsymbol{u}}_{c,N+1}\right)$, $\boldsymbol{g}^{vel}_{c,N+1}\left(\tilde{\boldsymbol{u}}_{c,N+1}\right)$, and $\boldsymbol{g}^{acc}_{c,N+1}\left(\tilde{\boldsymbol{u}}_{c,N+1}\right)$ are expanded in a Taylor series with respect to $\tilde{\boldsymbol{u}}_{c,N+1}$. As expansion point, we choose $\tilde{\boldsymbol{u}}^p_{c,N+1}$. Neglecting the higher order terms, a Taylor series expansion of $\boldsymbol{g}^{pos}_{c,N+1}\left(\tilde{\boldsymbol{u}}_{c,N+1}\right)$, $\boldsymbol{g}^{vel}_{c,N+1}\left(\tilde{\boldsymbol{u}}_{c,N+1}\right)$, and $\boldsymbol{g}^{acc}_{c,N+1}\left(\tilde{\boldsymbol{u}}_{c,N+1}\right)$ yields the linearized coupling conditions

$$\boldsymbol{g}^{pos,linear}_{c,N+1}\left(\tilde{\boldsymbol{u}}_{c,N+1}\right) := \boldsymbol{g}^{pos}_{c,N+1}\left(\tilde{\boldsymbol{u}}^p_{c,N+1}\right) + \left.\frac{\partial \boldsymbol{g}^{pos}_{c,N+1}}{\partial \tilde{\boldsymbol{u}}_{c,N+1}}\right|_{\tilde{\boldsymbol{u}}^p_{c,N+1}} \cdot \left(\tilde{\boldsymbol{u}}_{c,N+1} - \tilde{\boldsymbol{u}}^p_{c,N+1}\right) = \boldsymbol{0}, \tag{72a}$$

$$\boldsymbol{g}^{vel,linear}_{c,N+1}\left(\tilde{\boldsymbol{u}}_{c,N+1}\right) := \boldsymbol{g}^{vel}_{c,N+1}\left(\tilde{\boldsymbol{u}}^p_{c,N+1}\right) + \left.\frac{\partial \boldsymbol{g}^{vel}_{c,N+1}}{\partial \tilde{\boldsymbol{u}}_{c,N+1}}\right|_{\tilde{\boldsymbol{u}}^p_{c,N+1}} \cdot \left(\tilde{\boldsymbol{u}}_{c,N+1} - \tilde{\boldsymbol{u}}^p_{c,N+1}\right) = \boldsymbol{0}, \tag{72b}$$

$$\boldsymbol{g}^{acc,linear}_{c,N+1}\left(\tilde{\boldsymbol{u}}_{c,N+1}\right) := \boldsymbol{g}^{acc}_{c,N+1}\left(\tilde{\boldsymbol{u}}^p_{c,N+1}\right) + \left.\frac{\partial \boldsymbol{g}^{acc}_{c,N+1}}{\partial \tilde{\boldsymbol{u}}_{c,N+1}}\right|_{\tilde{\boldsymbol{u}}^p_{c,N+1}} \cdot \left(\tilde{\boldsymbol{u}}_{c,N+1} - \tilde{\boldsymbol{u}}^p_{c,N+1}\right) = \boldsymbol{0}. \tag{72c}$$

- Solving the linearized coupling conditions (72a) for the coupling variables yields the corrected coupling variables

$$\tilde{\boldsymbol{u}}_{c,N+1}^{pos} = \tilde{\boldsymbol{u}}_{c,N+1}^{p} - \boldsymbol{G}^{pos^{-1}} \cdot \boldsymbol{g}_{c,N+1}^{pos}\left(\tilde{\boldsymbol{u}}_{c,N+1}^{p}\right) \quad \text{with} \quad \boldsymbol{G}^{pos} = \left.\frac{\partial \boldsymbol{g}_{c,N+1}^{pos}}{\partial \tilde{\boldsymbol{u}}_{c,N+1}}\right|_{\tilde{\boldsymbol{u}}_{c,N+1}^{p}} . \tag{73}$$

  Solving the linearized coupling conditions (72b) for the coupling variables yields the corrected coupling variables

$$\tilde{\boldsymbol{u}}_{c,N+1}^{vel} = \tilde{\boldsymbol{u}}_{c,N+1}^{p} - \boldsymbol{G}^{vel^{-1}} \cdot \boldsymbol{g}_{c,N+1}^{vel}\left(\tilde{\boldsymbol{u}}_{c,N+1}^{p}\right) \quad \text{with} \quad \boldsymbol{G}^{vel} = \left.\frac{\partial \boldsymbol{g}_{c,N+1}^{vel}}{\partial \tilde{\boldsymbol{u}}_{c,N+1}}\right|_{\tilde{\boldsymbol{u}}_{c,N+1}^{p}} . \tag{74}$$

  Solving the linearized coupling conditions (72c) for the coupling variables yields the corrected coupling variables

$$\tilde{\boldsymbol{u}}_{c,N+1}^{acc} = \tilde{\boldsymbol{u}}_{c,N+1}^{p} - \boldsymbol{G}^{acc^{-1}} \cdot \boldsymbol{g}_{c,N+1}^{acc}\left(\tilde{\boldsymbol{u}}_{c,N+1}^{p}\right) \quad \text{with} \quad \boldsymbol{G}^{acc} = \left.\frac{\partial \boldsymbol{g}_{c,N+1}^{acc}}{\partial \tilde{\boldsymbol{u}}_{c,N+1}}\right|_{\tilde{\boldsymbol{u}}_{c,N+1}^{p}} . \tag{75}$$

- Within the weighted multiplier method, the corrected coupling variables are calculated by the weighted average

$$\tilde{\boldsymbol{u}}_{c,N+1} = \frac{1}{1+a+b}\left(\tilde{\boldsymbol{u}}_{c,N+1}^{pos} + a \cdot \tilde{\boldsymbol{u}}_{c,N+1}^{vel} + b \cdot \tilde{\boldsymbol{u}}_{c,N+1}^{acc}\right) , \tag{76}$$

  where $a \geq 0$ and $b \geq 0$ are real-valued user-defined parameters (e.g. $a = b = 1$).

**Step 3: Corrector step**

- The corrector step is equivalent to method 1 in Sect. 3.3.1 with the only difference that $\tilde{\boldsymbol{u}}_{c,N+1}$ from Eq. (76) is used instead of $\tilde{\boldsymbol{u}}_{c,N+1}$ from Eq. (68).

#### 3.3.2.1 Semi-implicit index-3 co-simulation approach

For $a = b = 0$, method 2 is equivalent to the index-3 formulation of method 1.

#### 3.3.2.2 Semi-implicit index-2 co-simulation approach

Choosing $a > 0$ and $b = 0$ yields a co-simulation approach on index-2 level. Applying the index-2 approach, evaluation of Eqs. (58) and (61) is not required. Moreover, only partial derivatives of the state variables with respect to the coupling variables have to be calculated (partial derivatives of the accelerations are not required).

#### 3.3.2.3 Semi-implicit index-1 co-simulation approach

Choosing $a > 0$ and $b > 0$ yields an index-1 co-simulation approach.

## 4 Numerical examples

In this section, both semi-implicit co-simulation methods are analyzed in detail with 3 numerical examples. We investigate the convergence, the numerical error and the stability behavior of the coupling schemes.

### 4.1 Linear 1-DOF oscillator

#### 4.1.1 Method 1: Semi-implicit co-simulation approach based on Baumgarte-stabilization

We consider again the linear 1-DOF oscillator of Sect. 2. Simulations have been accomplished with the following parameters: $m_1 = 1$, $m_2 = 2$, $c = c_1 = c_2 = 1000$, and $d = d_1 = d_2 = 10$. As initial conditions, we have set $x_{1,0} = x_{2,0} = 0$, $v_{1,0} = v_{2,0} = 100$, and $\lambda_{c,0} = 1000/3$. The two subsystems have been integrated with an implicit Runge-Kutta integrator (relative and absolute error tolerance $\varepsilon_{\text{rel}} = \varepsilon_{\text{abs}} = 1E-8$). Fig. 5 shows the time response $x_1(t)$ of the left mass, the residuum $x_2 - x_1$ and the Lagrange multiplier $\lambda_c(t)$ for the index-1 ($k = 0$ and $k = 1$), the index-2 ($k = 0$) and the index-3 ($k = 0$) approach. The simulations have been carried out with the Baumgarte parameters $\beta = 2E-3$, $\gamma = 1E-6$ and with the macro-step-size $H = 1E-3$.

The global error over the macro-step size is plotted in Fig. 6 for the index-1 ($k = 0$), the index-2 ($k = 0$) and the index-3 ($k = 0$) approach for three different sets of Baumgarte-parameters: $\beta = 2E-1$, $\gamma = 1E-2$; $\beta = 2E-2$, $\gamma = 1E-4$, and $\beta = 2E-3$, $\gamma = 1E-6$. As reference solution for calculating the global error, the analytical solution of Eq. (1) has

 

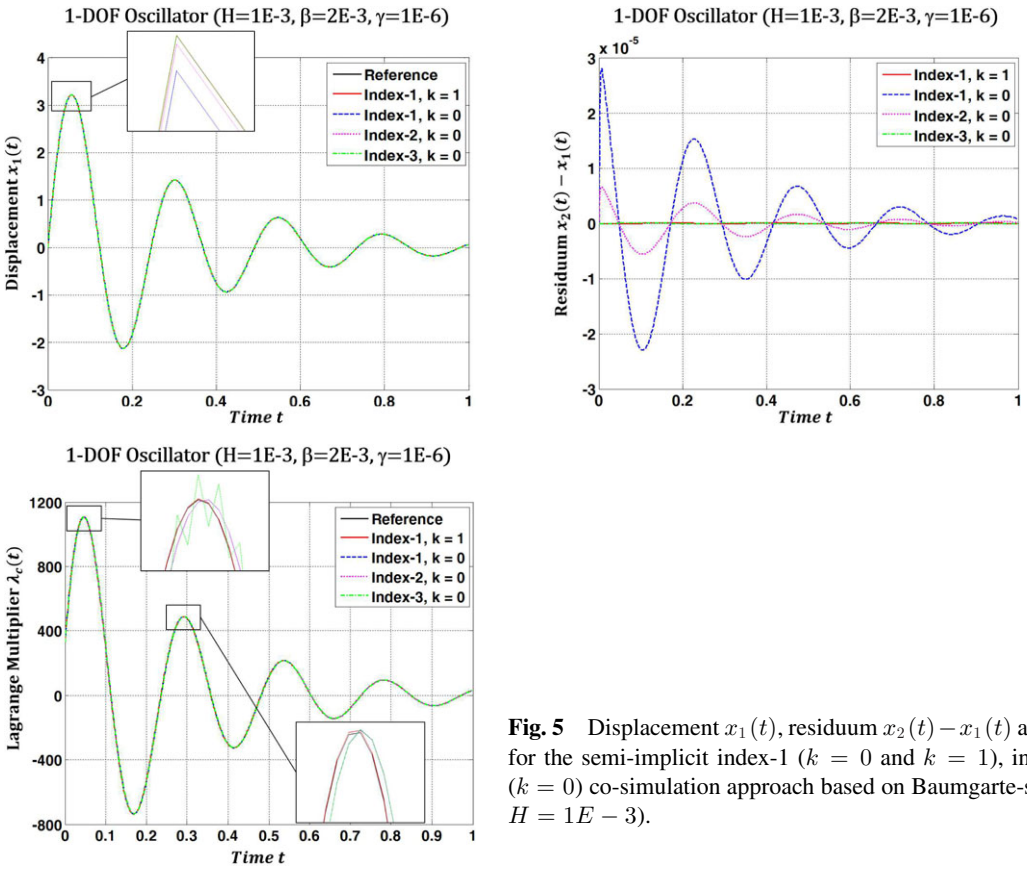


**Fig. 5** Displacement $x_1(t)$, residuum $x_2(t) - x_1(t)$ and Lagrange multiplier $\lambda_c(t)$ for the semi-implicit index-1 ($k = 0$ and $k = 1$), index-2 ($k = 0$), and index-3 ($k = 0$) co-simulation approach based on Baumgarte-stabilization (macro-step size $H = 1E - 3$).

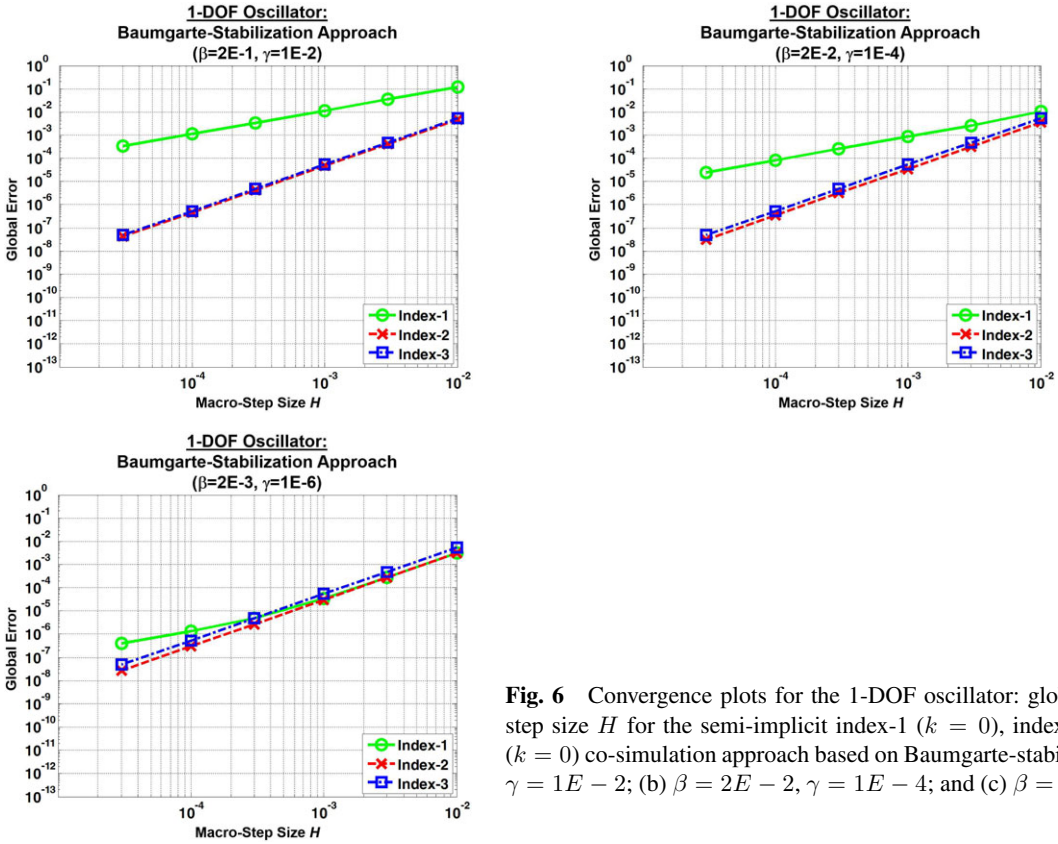


**Fig. 6** Convergence plots for the 1-DOF oscillator: global error over the macro-step size $H$ for the semi-implicit index-1 ($k = 0$), index-2 ($k = 0$), and index-3 ($k = 0$) co-simulation approach based on Baumgarte-stabilization. (a) $\beta = 2E - 1$, $\gamma = 1E - 2$; (b) $\beta = 2E - 2$, $\gamma = 1E - 4$; and (c) $\beta = 2E - 3$, $\gamma = 1E - 6$.

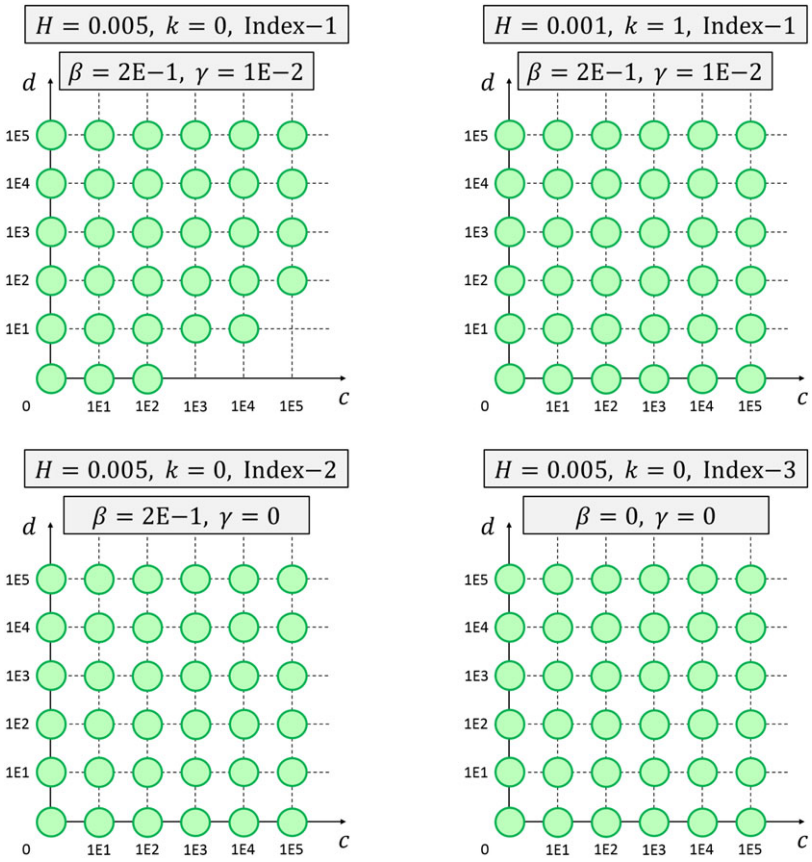


**Fig. 7** Stable co-simulations for different stiffness coefficients $c$ and damping coefficients $d$ for the semi-implicit index-1 ($k = 0$ and $k = 1$), index-2 ($k = 0$), and index-3 ($k = 0$) co-simulation approach based on Baumgarte-stabilization ($\beta = 2E - 1$, $\gamma = 1E - 2$).

been used. It can be seen that for the index-2 and index-3 approach, the global error converges with $\mathcal{O}(H^2)$. In case of the index-1 approach, the global error is increased and the order of convergence is decreased, especially for larger Baumgarte parameters.

The stability behavior of the coupling approach on index-1 ($k = 0$ and $k = 1$), index-2 ($k = 0$) and index-3 ($k = 0$) level is illustrated by means of stability plots. Therefore, co-simulations have been accomplished for different values of $c$ and $d$ ($H = 5E - 3$ for $k = 0$ and $H = 1E - 3$ for $k = 1$). In the plots, stable simulations are indicated with a "O". Fig. 7 depicts stability plots for the Baumgarte-parameters $\beta = 2E - 1$, $\gamma = 1E - 2$. Corresponding plots for $\beta = 2E - 2$,

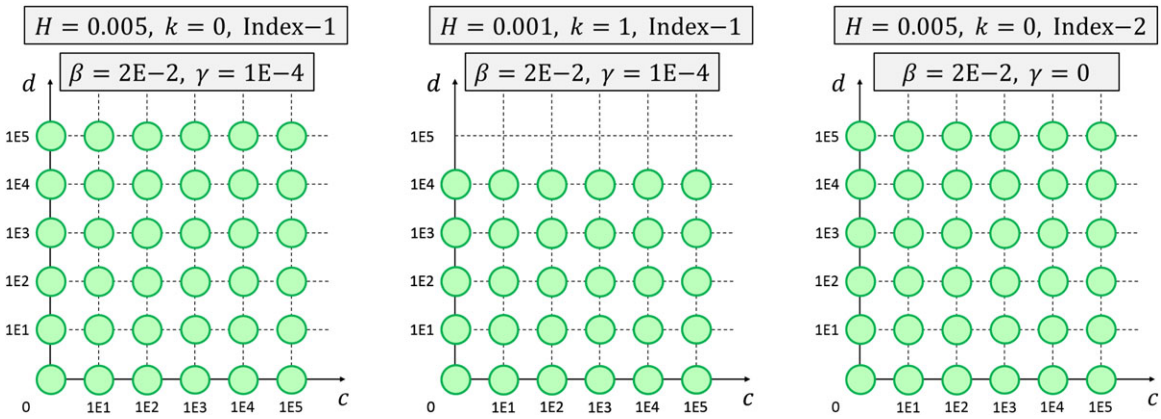


**Fig. 8** Stable co-simulations for different stiffness coefficients $c$ and damping coefficients $d$ for the semi-implicit index-1 ($k = 0$ and $k = 1$) and index-2 ($k = 0$) co-simulation approach based on Baumgarte-stabilization ($\beta = 2E - 2$, $\gamma = 1E - 4$).

 

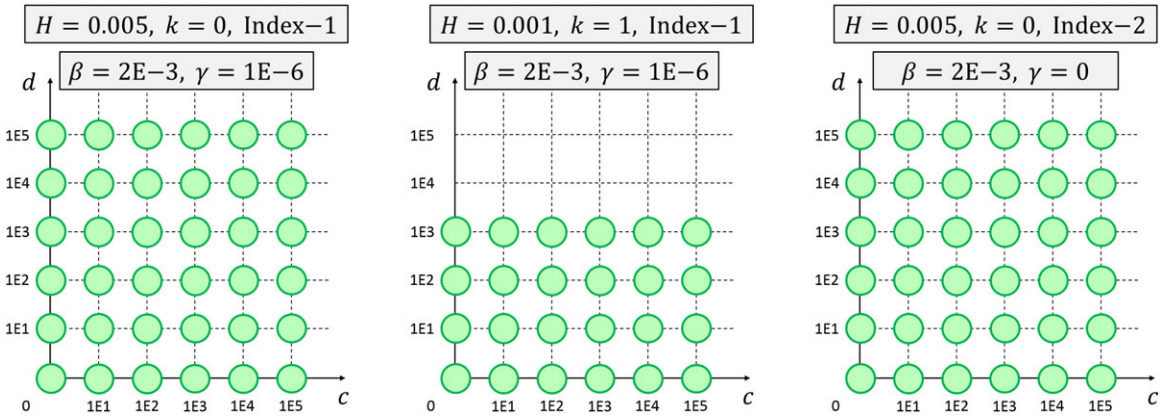


**Fig. 9** Stable co-simulations for different stiffness coefficients $c$ and damping coefficients $d$ for the semi-implicit index-1 ($k = 0$ and $k = 1$) and index-2 ($k = 0$) co-simulation approach based on Baumgarte-stabilization ($\beta = 2E - 3$, $\gamma = 1E - 6$).

$\gamma = 1E - 4$ and $\beta = 2E - 3$, $\gamma = 1E - 6$ are shown in Fig. 8 and Fig. 9. Using larger Baumgarte parameters, the index-1 co-simulation approach becomes unstable for larger values of $c$, see Fig. 7a. This region of instability vanishes if the macro-step size is reduced and the approximation order is increased, see Fig. 7b. The index-2 and index-3 co-simulation approaches are stable in the considered parameter range, see Fig. 7c and 7d. Choosing smaller Baumgarte parameters, one can observe from Fig. 8 and Fig. 9 that the co-simulation may become unstable for larger values of $d$. It should be stressed that the numerical subsystem integration has almost no influence on the stability of the co-simulation, since the subsystems have been integrated with very small error tolerances. Hence, replacing the numerical subsystem integration by an analytical integration yields the same plots.

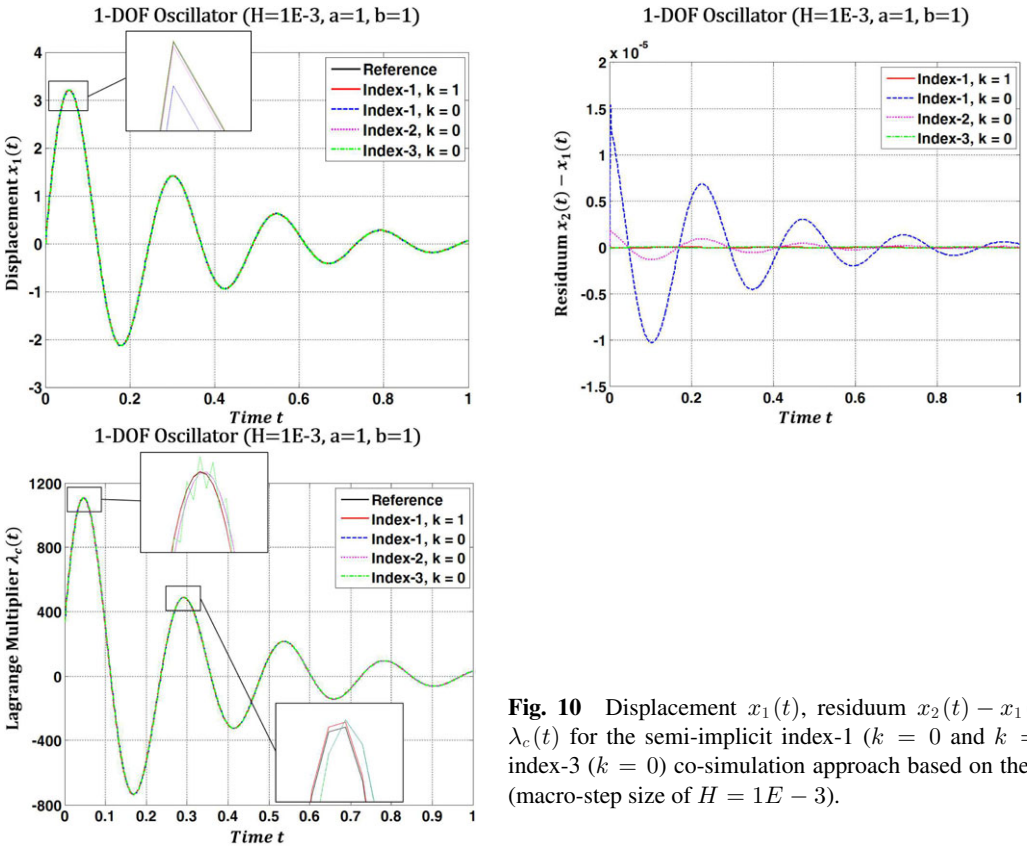


**Fig. 10** Displacement $x_1(t)$, residuum $x_2(t) - x_1(t)$ and Lagrange multiplier $\lambda_c(t)$ for the semi-implicit index-1 ($k = 0$ and $k = 1$), index-2 ($k = 0$), and index-3 ($k = 0$) co-simulation approach based on the weighted multiplier method (macro-step size of $H = 1E - 3$).

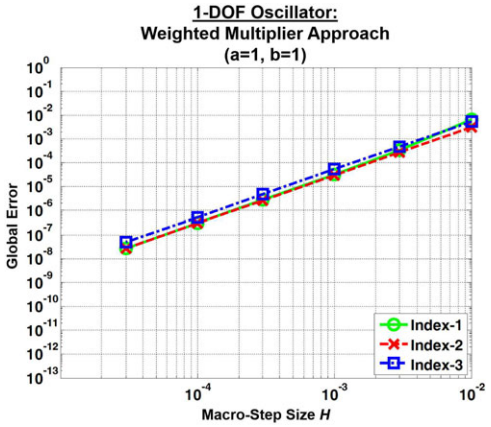


**Fig. 11** Convergence plots for the 1-DOF oscillator: global error over macro-step size $H$ for the semi-implicit index-1 ($k = 0$), index-2 ($k = 0$), and index-3 ($k = 0$) co-simulation approach based on the weighted multiplier method.

### 4.1.2 Method 2: Semi-implicit co-simulation approach based on weighted multipliers

The linear 1-DOF oscillator is now simulated with the weighted multiplier approach. In Fig. 10, the displacement $x_1(t)$ of the left mass, the residuum $x_2 - x_1$ and the Lagrange multiplier $\lambda_c(t)$ are plotted for the index-1 ($a = 1$, $b = 1$; $k = 0$ and $k = 1$), the index-2 ($a = 1$, $b = 0$; $k = 0$) and the index-3 ($a = 0$, $b = 0$; $k = 0$) approach for a macro-step-size of $H = 1E - 3$. Note again that the index-3 approach of method 2 is equivalent to the index-3 formulation of method 1.

Figure 11 depicts the global error over the macro-step size for the index-1 ($a = 1$, $b = 1$; $k = 0$), the index-2 ($a = 1$, $b = 0$; $k = 0$), and the index-3 ($a = 0$, $b = 0$; $k = 0$) approach. The global error converges with $\mathcal{O}(H^2)$ for the index-1, index-2, and index-3 approach. Order reduction effects for the index-1 method – as in the case of the Baumgarte approach – are not observed for the considered parameters $a$ and $b$.

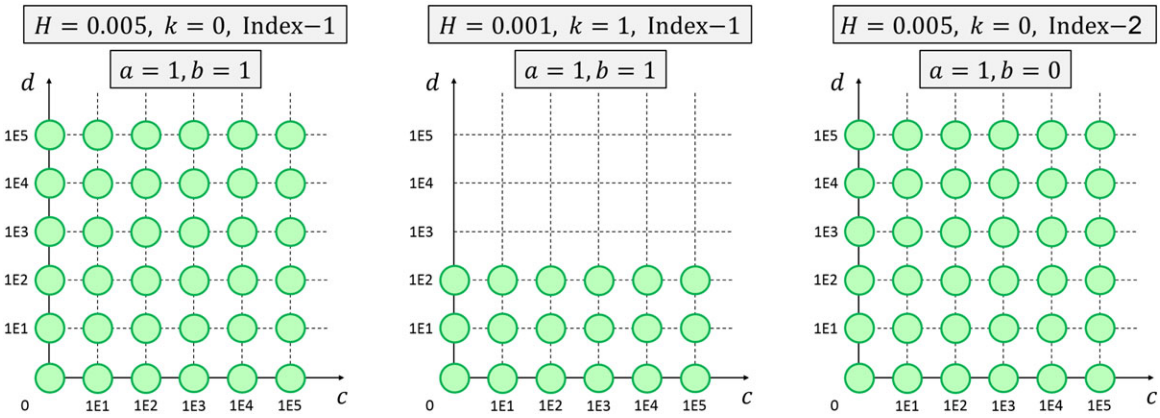


**Fig. 12** Stable co-simulations for different stiffness coefficients $c$ and damping coefficients $d$ for the semi-implicit index-1 ($k = 0$ and $k = 1$) and index-2 ($k = 0$) co-simulation approach based on the weighted multiplier method.

The stability behavior of the weighted multiplier approach on index-1 ($k = 0$ and $k = 1$) and index-2 ($k = 0$) level is illustrated in Fig. 12. As in Sect. 4.1.1, co-simulations have been accomplished for different values of $c$ and $d$ ($H = 5E - 3$ for $k = 0$ and $H = 1E - 3$ for $k = 1$). Stable simulations are indicated with a "O". The stability plots are similar to the plots in Sect. 4.1.1. As for the Baumgarte approach, unstable co-simulations are detected for larger values of $d$ in case of the index-1 method with $k = 1$, see Fig. 12b.

### 4.1.3 Comparison with explicit coupling approach

The 1-DOF oscillator is finally calculated with the explicit coupling method of [16]. This method is based on an index-1 approach, uses constant approximation ($k = 0$) and requires the specification of one user-defined parameter ($\mu_B$). Convergence and stability plots for different values of $\mu_B$ are shown in Fig. 13 and Fig. 14. It can be seen that the accuracy of the explicit approach is improved for smaller values of $\mu_B$. However, the smaller $\mu_B$ is chosen, the more the stable region is reduced. Compared with the semi-implicit methods, one observes that the numerical error is larger and the region of stability is smaller for the explicit approach.

 

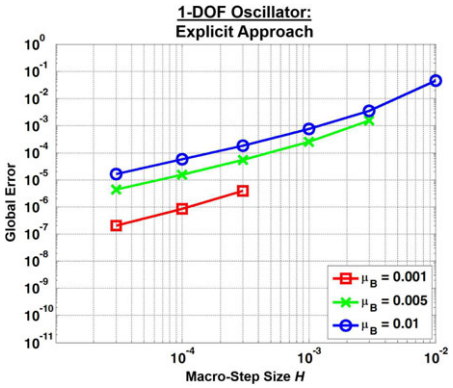


**Fig. 13** Convergence plots for the 1-DOF oscillator: global error over macro-step size $H$ for the explicit index-1 co-simulation approach of [16].

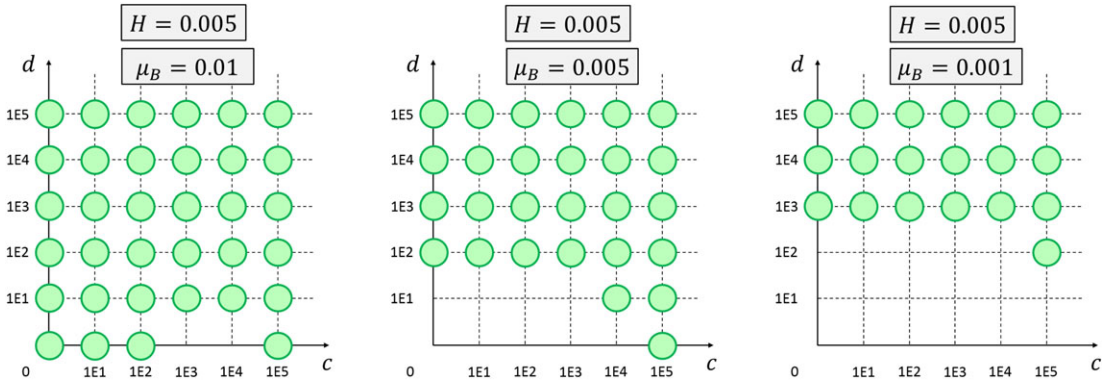


**Fig. 14** Stable co-simulations for different stiffness coefficients $c$ and damping coefficients $d$ for the explicit index-1 co-simulation approach of [16].

### 4.2 Double pendulum

#### 4.2.1 Method 1: Semi-implicit co-simulation approach based on Baumgarte-stabilization

Next, we investigate the planar double pendulum (masses $m_1 = m_2 = 1$, moments of inertia $J_1 = J_2 = 1/12$, lengths $l_1 = l_2 = 1$) illustrated in Fig. 15. Link 1 (subsystem 1) is connected to ground by a revolute joint and a torsional spring/damper-system (spring constant $c_\varphi = 500$, damping coefficient $d_\varphi = 50$). The spring is assumed to be stress-free for $\varphi_1 = \pi/4$. Link 2 (subsystem 2) is coupled to link 1 by an atpoint joint, which is in the planar case equivalent to a revolute joint. Gravity is acting in negative y-direction ($g = 9.81$). As initial conditions, we have set $\varphi_{1,0} = \pi/4$, $\varphi_{2,0} = -\pi/4$, $\dot{\varphi}_{1,0} = \dot{\varphi}_{2,0} = 0$. An implicit Runge-Kutta method (relative and absolute error tolerance $\varepsilon_{\mathrm{rel}} = \varepsilon_{\mathrm{abs}} = 1E-8$) has been applied for integrating the subsystems. It should be pointed out that subsystem 1 is a DAE system, which has been solved with the MAPLE solver "rosenbrock_dae". Fig. 16 illustrates the angles $\varphi_1(t)$ and $\varphi_2(t)$ as well as the Lagrange multipliers

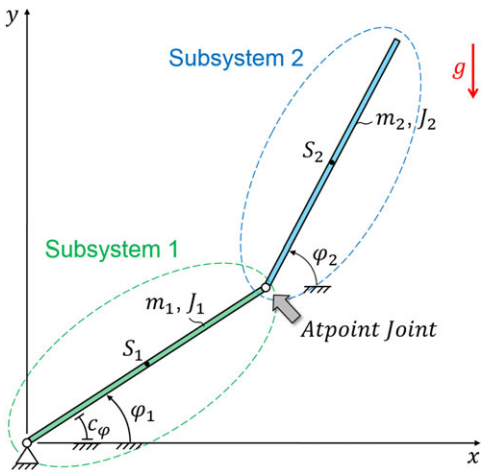


**Fig. 15** Double pendulum: interpretation as two links coupled by an atpoint joint.

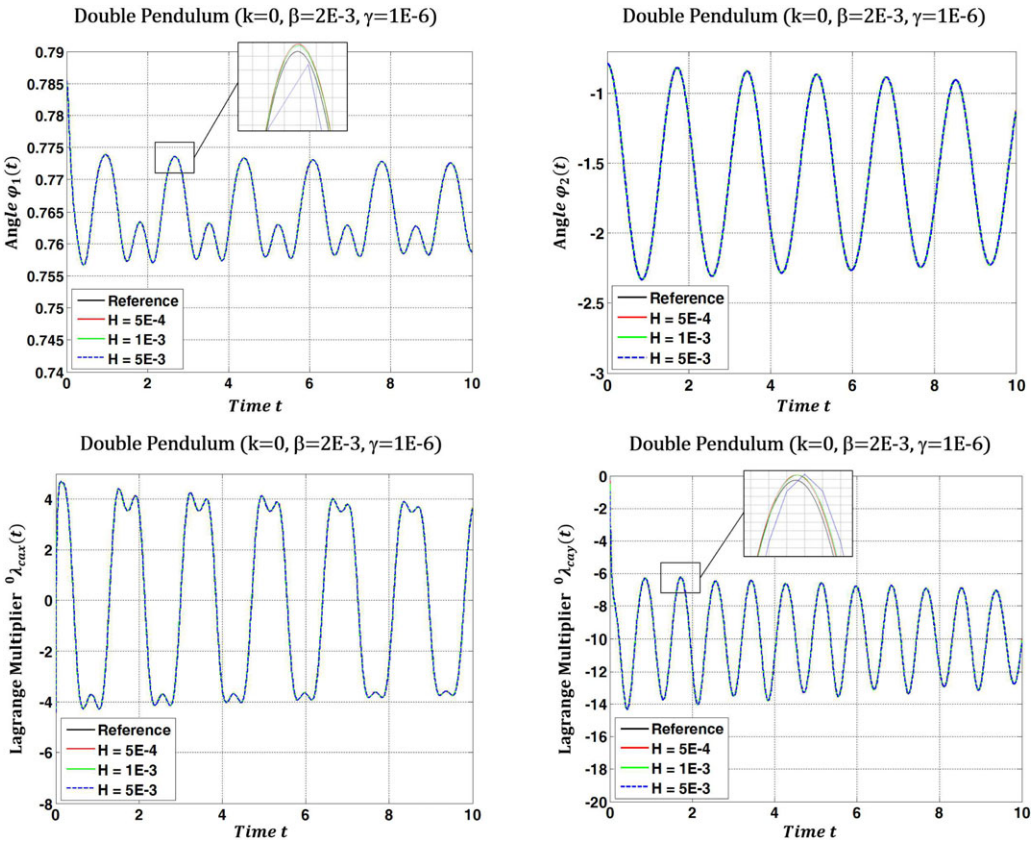


**Fig. 16** Co-simulation results based on semi-implicit Baumgarte approach for the double pendulum: angles $\varphi_1(t)$ and $\varphi_2(t)$, Lagrange multipliers $\lambda_{ca_x}(t)$ and $\lambda_{ca_y}(t)$ for different macro-step sizes $H$.

$\lambda_{ca_x}(t)$ and $\lambda_{ca_y}(t)$ for different macro-step sizes $H$ (index-1; $\beta = 2E-3$, $\gamma = 1E-6$; $k = 0$). The reference solution has been computed numerically with a monolithic model. The plots show that the co-simulation yields accurate results. The convergence of the method can clearly be seen.

### 4.2.2 Method 2: Semi-implicit co-simulation approach based on weighted multipliers

The double pendulum is now simulated with the weighted multiplier approach (index-1; $a = 1$, $b = 1$; $k = 0$). The results can be seen in Fig. 17. As in the previous section, accuracy and convergence of the co-simulation can clearly be observed.

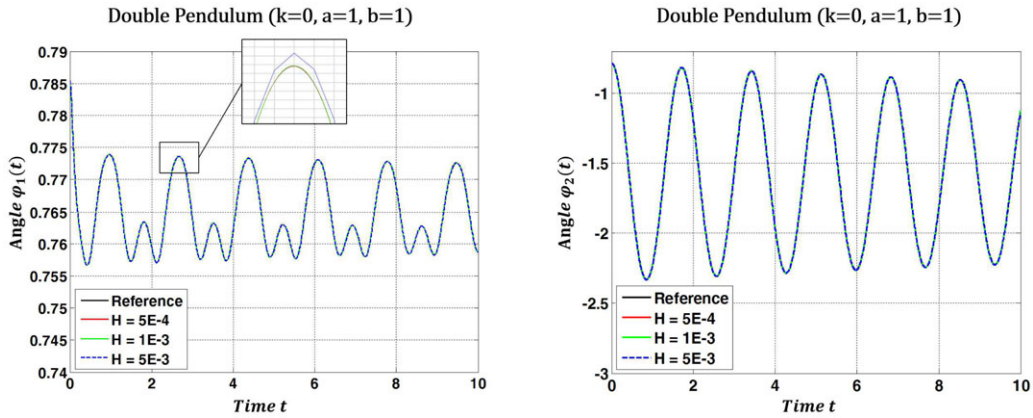


**Fig. 17** Co-simulation results based on the weighted multiplier method for the double pendulum: angles $\varphi_1(t)$ and $\varphi_2(t)$, Lagrange multipliers $\lambda_{ca_x}(t)$ and $\lambda_{ca_y}(t)$ for different macro-step sizes $H$.

 

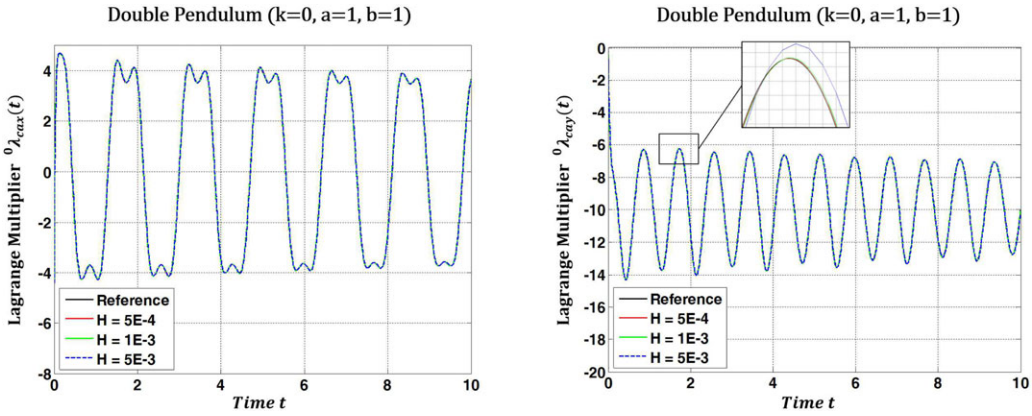


**Fig. 17** (Continued).

### 4.3 Slider-crank mechanism

#### 4.3.1 Method 1: Semi-implicit co-simulation approach based on Baumgarte-stabilization

The slider-crank mechanism shown in Fig. 18 is considered as third example. Link 1 (representing subsystem 1) and link 2 (representing subsystem 2) are both connected to ground by a revolute joint. The two links are coupled by an inplane joint. Gravity is acting in negative y-direction ($g = 9.81$). The simulations have been accomplished with the subsequent parameters: $m_1 = \sqrt{2}$, $m_2 = 2$, $J_1 = \sqrt{2}/6$, $J_2 = 2/3$, $l_1 = \sqrt{2}$, $l_2 = 2$. As initial conditions, we have set $\varphi_{1,0} = \pi/4$, $\varphi_{2,0} = \pi/2$, $\dot{\varphi}_{1,0} = \dot{\varphi}_{2,0} = 0$. As subsystem solver, an implicit Runge-Kutta integrator (relative and absolute error tolerance $\varepsilon_{\mathrm{rel}} = \varepsilon_{\mathrm{abs}} = 1E-8$) has been used. Simulation results are collected in Fig. 19, which shows the angles

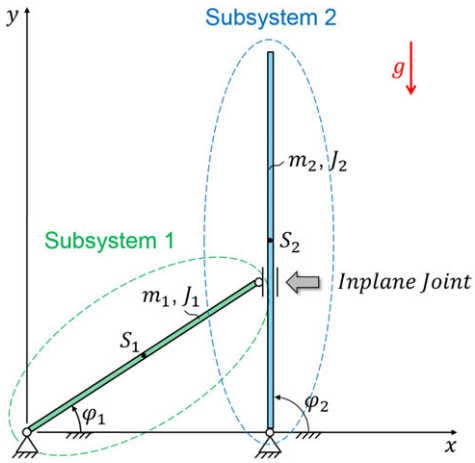


**Fig. 18** Slider-crank mechanism: interpretation as two links coupled by an inplane joint.

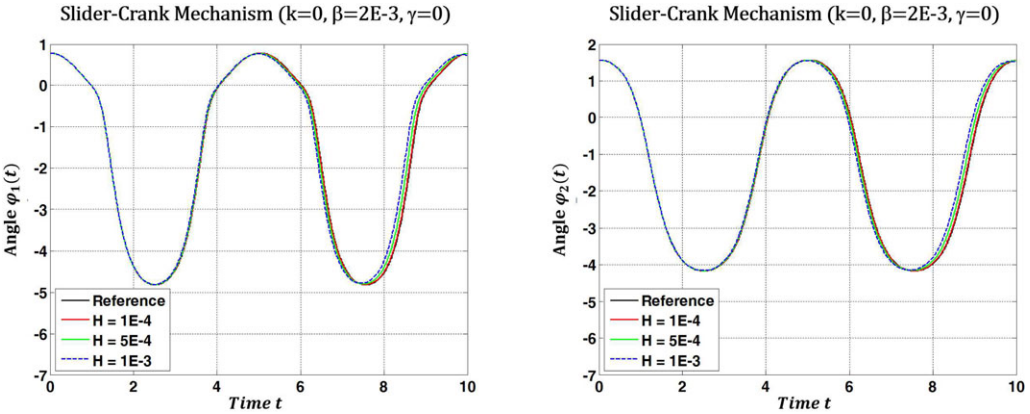


**Fig. 19** Co-simulation results based on semi-implicit Baumgarte approach for the slider-crank mechanism: angles $\varphi_1(t)$ and $\varphi_2(t)$, Lagrange multiplier $\lambda_{cd}(t)$, total energy $E_{total}(t)$ for different macro-step sizes $H$.

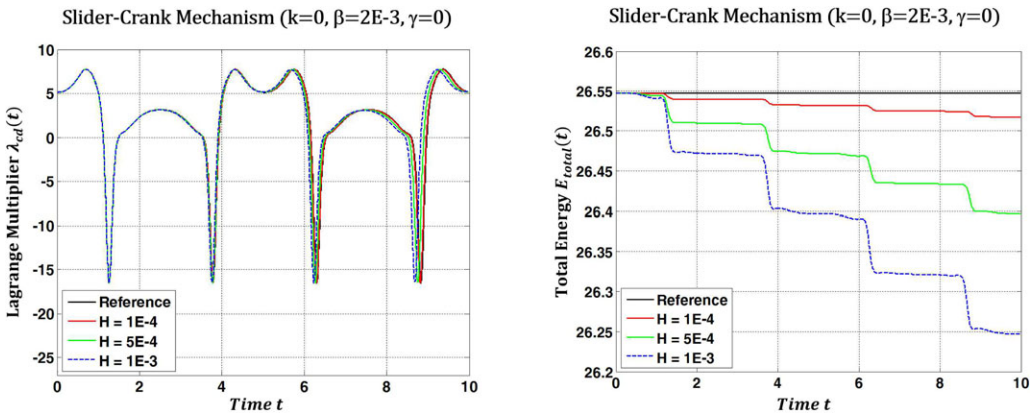


**Fig. 19** (Continued).

$\varphi_1(t)$ and $\varphi_2(t)$, the Lagrange multiplier $\lambda_{cd}(t)$ as well as the total energy $E_{total}(t)$ of the system (kinetic plus potential energy) for different macro-step sizes $H$ (index-2; $\beta = 2E-3$, $\gamma = 0$; $k = 0$). The plots illustrate the convergence of the co-simulation method. Regarding Fig. 19d, the numerical dissipation introduced by the co-simulation can be seen for different macro-step sizes. Further simulations show that the numerical dissipation is significantly reduced if higher order approximation is used ($k > 0$).

### 4.3.2 Method 2: Semi-implicit co-simulation approach based on weighted multipliers

Simulation results for the slider-crank mechanism based on the weighted multiplier approach (index-2; $a = 1$, $b = 0$; $k = 0$) are arranged in Fig. 20. The plots are almost identical with the corresponding plots in the previous section.

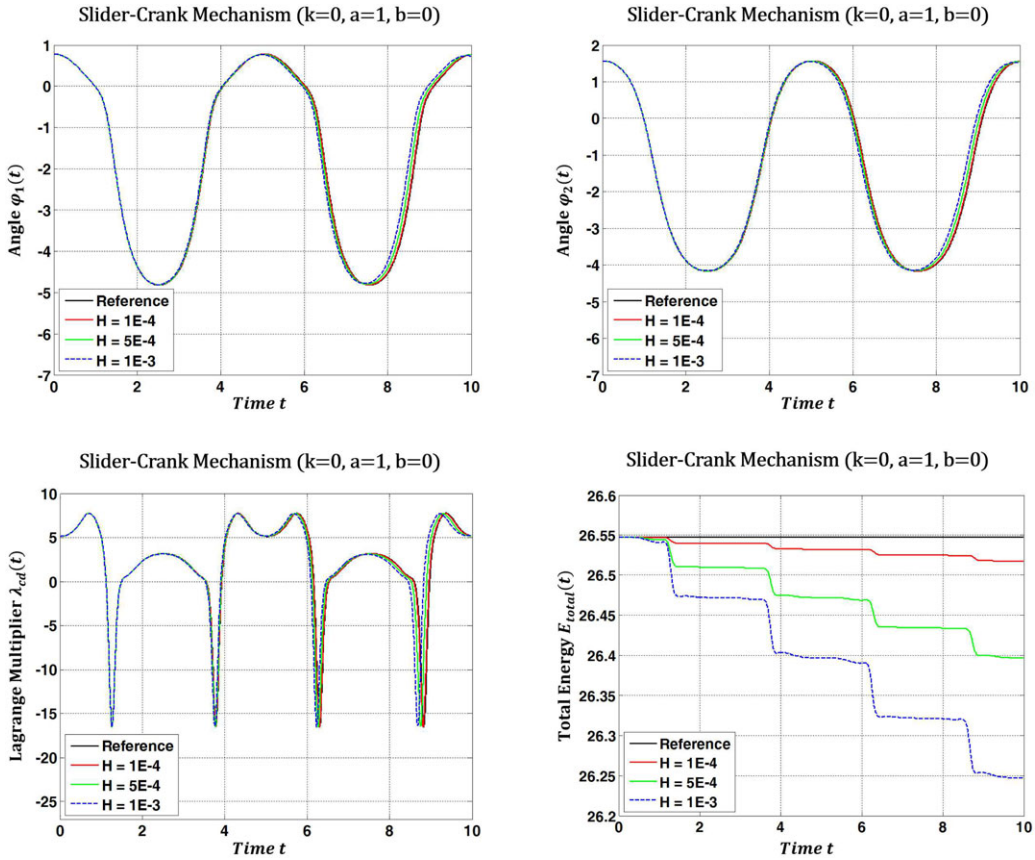


**Fig. 20** Co-simulation results based on the weighted multiplier method for the slider-crank mechanism: angles $\varphi_1(t)$ and $\varphi_2(t)$, Lagrange multiplier $\lambda_{cd}(t)$, total energy $E_{total}(t)$ for different macro-step sizes $H$.

 

### 4.4 Comparison of both methods

A direct comparison of both methods is difficult, since the performance of both methods strongly depends on the parameters $\beta$, $\gamma$ and $a$, $b$. Concerning simulation time and numerical efficiency, both methods are almost identical, since both methods use the same predictor variables and the same partial derivatives. Comparing the simulation results of method 1 and 2, certain differences can be observed. Regarding the convergence plots for the Baumgarte approach, it is interesting to notice that – especially for larger Baumgarte parameters – the global error for the index-1 formulation is larger than for the index-2 and index-3 formulations, see Fig. 6. Using the obvious and intuitive parameters $a = 1$ and $b = 1$, a reduction of the global error is not observed for the index-1 formulation, see Fig. 11. For the considered parameter range of the stiffness and damping coefficients, stability behavior of the two methods is quite similar, at least for the case that smaller values of $\beta$ and $\gamma$ are used. In future work, a rigorous stability analysis has to be carried out in order to compare both methods in more detail. A further interesting point to be investigated in future work is the question, how the methods perform if a variable macro-step size is applied. From the practical point of view, the proper choice of the parameters $a$, $b$ and $\beta$, $\gamma$ is an important issue. Choosing appropriate parameters $a$ and $b$ might be – at least to the authors' opinion – somewhat easier, since the physical interpretation of $a$ and $b$ is quite intuitive.

## 5 Conclusions

Co-simulation methods based on a predictor/corrector approach for coupling two arbitrary mechanical systems by rigid joints, i.e. by algebraic constraints, have been analyzed. Two methods have been presented and formulations on index-1, index-2 and index-3 level have been investigated. Within this paper, the macro-step size (communication-step size) has assumed to be constant. Depending on the subsystem parameters, the macro-step size and the degree of the approximation polynomials, both methods showed stable and convergent simulation results. In our numerical tests, the index-1 formulation yielded stable results for constant ($k = 0$), linear ($k = 1$) and quadratic ($k = 2$) approximation polynomials (the case $k > 2$ has not been examined). The index-2 formulation showed stable simulations for constant and partly for linear polynomials. On index-3 level, the coupled simulation was stable for constant approximation. By repeating the corrector step several times, i.e. by performing a corrector iteration, full-implicit methods are obtained, which may further improve the simulation results. Using the predicted and the corrected variables, implementation of an error estimator for controlling the macro-step size can be realized in a straightforward manner. Besides the two predictor/corrector methods presented in this manuscript, a further method can simply be obtained by using the coupling equations on acceleration level and by applying a classical projection approach to avoid the drift effect [24].

## References

[1] J. Arnold, G. Einarsson, and W. Krueger, Multibody simulation of an oscillating aeroelastic wing model, NAFEMS Int. J. CFD Case Studies **8**, 5–18 (2009).
[2] M. Arnold, A. Carrarini, A. Heckmann, and G. Hippmann, Simulation Techniques for Multidisciplinary Problems in Vehicle System Dynamics, In: Computational Mechanics in Vehicle System Dynamics, Vol. 40 of Supplement to Vehicle System Dynamics, edited by M. Valasek (Taylor & Francis, London, 2004), pp. 17–36.
[3] M. Arnold, Stability of sequential modular time integration methods for coupled multibody system models, J. Comput. Nonlinear Dyn. **5**, 1–9 (2010).
[4] J. Baumgarte, Stabilization of constraints and integrals of motion in dynamical systems, Comput. Methods Appl. Mech. Eng. **1**, 1–16 (1972).
[5] K. Burrage, Parallel and Sequential Methods for Ordinary Differential Equations, Numerical Mathematics and Scientific Computation (Oxford University Press, Oxford, 1995).
[6] M. Busch, A. Arnold, A. Heckmann, and S. Dronka, Interfacing SIMPACK to Modelica/Dymola for multi-domain vehicle system simulations, SIMPACK News **11**, 1–3 (2007).
[7] M. Busch, Zur effizienten Kopplung von Simulationsprogrammen (On the Efficient Coupling of Simulation Codes), PhD Thesis (Kassel University Press, University of Kassel, 2012), ISBN-13: 978-3862192960.
[8] M. Busch and B. Schweizer, Coupled simulation of multibody and finite element systems: an efficient and robust semi-implicit coupling approach, Arch. Appl. Mech. **82**(6), 723–741 (2012).
[9] M. Busch, and B. Schweizer, Numerical Stability and Accuracy of Different Co-simulation Techniques: Analytical Investigations Based on a 2-DOF Test Model, In: Proceedings of The 1st Joint International Conference on Multibody System Dynamics, Lappeenranta, 2010 (Lapeenranta Technical University, Lapeenranta, 2010).
[10] M. Busch, and B. Schweizer, An Explicit Approach for Controlling the Macro-Step Size of Co-simulation Methods, In: Proceedings of The 7th European Nonlinear Dynamics, ENOC 2011, 24–29 July 2011, Rome, Italy (Sapienza University, Rome, 2011).
[11] V. Carstens, R. Kemme, and S. Schmitt, Coupled simulation of flow-structure interaction in turbomachinery, Aerospace Sci. Technol. **7**, 298–306 (2003).

 

[12] S. Dietz, G. Hippmann, and G. Schupp, Interaction of Vehicles and Flexible Tracks by Co-simulation of Multibody Vehicle Systems and Finite Element Track Models, In: The Dynamics of Vehicles on Roads and on Tracks, Vol. 37 of Supplement to Vehicle System Dynamics, edited by H. True (Swets & Zeitlinger, Lisse, 2003), pp. 17–36.
[13] M. Crow and M. Ilic, The parallel implementation of the waveform relaxation method for transient stability simulations, IEEE Trans. Power Syst. **5**, 922–932 (1990).
[14] M. Friedrich and H. Ulbrich, A Parallel Co-simulation for Mechatronic Systems, In: Proceedings of The 1st Joint International Conference on Multibody System Dynamics, Lappeenranta, (Lapeenranta Technical University, Lapeenranta, 2010).
[15] M. Guenther and P. Rentrop, Multirate row methods and latency of electric circuits, Appl. Numer. Math. **13**, 83–102 (1999).
[16] B. Gu and H. H. Asada, Co-simulation of algebraically coupled dynamic subsystems without disclosure of proprietary subsystem models, J. Dyn. Syst. Meas. Control **126**, 1–13 (2004), DOI: 10.1115/1.1648307.
[17] E. J. Haug, Computer-Aided Kinematics and Dynamics of Mechanical Systems, (Allyn and Bacon, Boston, 1989).
[18] S. Helduser, M. Stuewing, S. Liebig, and S. Dronka, Development of Electro-Hydraulic Actuators Using Linked Simulation and Hardware-in-the-Loop Technology, In: Power Transmission and Motion Control 2001, Bath, UK, edited by C. Burrows and K. Edge (University of Bath, Bath, 2001), pp. 49–56.
[19] G. Hippmann, M. Arnold, and M. Schittenhelm, Efficient Simulation of Bush and Roller Chain Drives, In: Proceedings of EC-COMAS Thematic Conference on Advances in Computational Multibody Dynamics, Madrid, edited by J. Goicolea, J. Cuadrado, and J. G. Orden, 2005, pp. 1–18, http://sim.mathematik.uni-halle.de.
[20] K. Jackson, A survey of parallel numerical methods for initial value problems for ordinary differential equations, IEEE Trans. Magn. **27**, 3792–3797 (1991).
[21] R. Kübler and W. Schiehlen, Two methods of simulator coupling, Math. Comput. Model. Dyn. Syst. **6**, 93–113 (2000).
[22] E. Lelarasmee, A. Ruehli, and A. Sangiovanni-Vincentelli, The waveform relaxation method for time domain analysis of large scale integrated circuits, IEEE Trans. CAD IC Syst. **1**, 131–145 (1982).
[23] R. Schmoll and B. Schweizer, Co-Simulation of Multibody and Hydraulic Systems: Comparison of Different Coupling Approaches, MULTIBODY DYNAMICS 2011, ECCOMAS Thematic Conference, edited by J. C. Samin and P. Fisette, Brussels, Belgium, 4–7 July, 2011 (UCL, Louvain-la-Neuve, 2011) pp. 1–13.
[24] B. Schweizer and D. Lu, Co-Simulation Methods for Solver Coupling with Algebraic Constraints: Semi-Implicit Coupling Techniques, In: Proceedings of The 3rd Joint International Conference on Multibody System Dynamics and The 7th Asian Conference on Multibody Dynamics, IMSD 2014, ACMD 2014, Bexco, Busan, Korea, June 30–July 3, (KSME, Busan, 2014).
[25] F. Tseng and G. Hulbert, Network-Distributed Multibody Dynamics Simulation-Gluing Algorithm, in: Advances in Computational Multibody Dynamics, edited by J. Ambrósio and W. Schiehlen (IDMEC/IST Lisbon, Portugal, 1999), pp. 521–540.
[26] O. Vaculin, W. R. Krueger, and M. Valasek, Overview of coupling of multibody and control engineering tools, Vehicle Syst. Dyn. **41**, 415–429 (2004).
[27] A. Verhoeven, E. J.W. ter Maten, R. M. M. Mattheij, and B. Tasi'z, BDF stability analysis of the BDF slowest-first multirate methods, Int. J. Comput. Math. **84**, 895–923 (2007).
[28] S. Wuensche, C. Clauß, P. Schwarz, and F. Winkler, Electro-thermal circuit simulation using simulator coupling, IEEE Trans. Very Large Scale Integr. (VLSI) Syst. **5**, 277–282 (1997).

 